Measurement of $D^0-\bar{D}^0$ mixing and search for CP violation with $D^0 \to K^+\pi^-$ decays

R. Aaij *et al.*[*]
(LHCb Collaboration)

(Received 30 July 2024; accepted 16 October 2024; published 3 January 2025)

A measurement of the time-dependent ratio of the $D^0 \to K^+\pi^-$ to $\bar{D}^0 \to K^+\pi^-$ decay rates is reported. The analysis uses a sample of proton-proton collisions corresponding to an integrated luminosity of 6 fb^{-1} recorded by the LHCb experiment from 2015 through 2018 at a center-of-mass energy of 13 TeV. The D^0 meson is required to originate from a $D^*(2010)^+ \to D^0\pi^+$ decay, such that its flavor at production is inferred from the charge of the accompanying pion. The measurement is performed simultaneously for the $K^+\pi^-$ and $K^-\pi^+$ final states, allowing both mixing and CP-violation parameters to be determined. The value of the ratio of the decay rates at production is determined to be $R_{K\pi} = (343.1 \pm 2.0) \times 10^{-5}$. The mixing parameters are measured to be $c_{K\pi} = (51.4 \pm 3.5) \times 10^{-4}$ and $c'_{K\pi} = (13 \pm 4) \times 10^{-6}$, where $\sqrt{R_{K\pi}}c_{K\pi}$ is the linear coefficient of the expansion of the ratio as a function of decay time in units of the D^0 lifetime, and $c'_{K\pi}$ is the quadratic coefficient, both averaged between the $K^+\pi^-$ and $K^-\pi^+$ final states. The precision is improved relative to the previous best measurement by approximately 60%. No evidence for CP violation is found.

DOI: 10.1103/PhysRevD.111.012001

I. INTRODUCTION

Flavor-changing neutral currents (FCNCs) and violation of charge-parity (CP) symmetry in charm-hadron decays are strongly suppressed by the Glashow-Iliopoulous-Maiani mechanism [1,2] and by the smallness of the elements of the Cabibbo-Kobayashi-Maskawa (CKM) matrix [3,4] connecting the first two generations of quarks with the third. As a result, measurements of these processes can provide precise null tests of the Standard Model (SM) [5]. The ultimate precision of these tests, however, is limited by theoretical uncertainties on contributions from long-distance quantum-chromodynamics (QCD), as reviewed in Refs. [6–9]. Additional measurements are needed both to improve knowledge of the size of these small effects, some of which are yet to be observed, and to help clarify the magnitude of long-distance QCD contributions.

The decay $D^0(t) \to K^+\pi^-$, where $D^0(t)$ denotes the state of a neutral charm meson, at proper time t, that was produced in the D^0 flavor eigenstate at $t = 0$, is an excellent candidate to study the effects described above (throughout this document, the inclusion of charge-conjugate processes is implied unless stated otherwise). This process receives contributions from interfering amplitudes of comparable magnitudes from the doubly Cabibbo-suppressed $D^0 \to K^+\pi^-$ decay and from the Cabibbo-favored $\bar{D}^0 \to K^+\pi^-$ decay following a $D^0-\bar{D}^0$ oscillation. Therefore, analysis of the time evolution of the decay rate provides sensitivity to the mixing parameters that determine the rate of $D^0-\bar{D}^0$ oscillations. These are $x_{12} \equiv 2|M_{12}|/\Gamma$ and $y_{12} \equiv |\Gamma_{12}|/\Gamma$ [10,11], defined from the 2×2 effective Hamiltonian governing the time evolution of the $D^0-\bar{D}^0$ system, $\boldsymbol{H} \equiv \boldsymbol{M} - \frac{i}{2}\boldsymbol{\Gamma}$, where Γ is the D^0 decay width.

The dependence of the measured quantities on the value of the D^0 lifetime can be greatly reduced by taking the ratio of the $D^0(t) \to K^+\pi^-$ rate with that of $\bar{D}^0(t) \to K^+\pi^-$, which is dominated by a Cabibbo-favored amplitude. This and the charge-conjugate ratio are defined as

$$R^+_{K\pi}(t) \equiv \frac{\Gamma(D^0(t) \to K^+\pi^-)}{\Gamma(\bar{D}^0(t) \to K^+\pi^-)},$$
$$R^-_{K\pi}(t) \equiv \frac{\Gamma(\bar{D}^0(t) \to K^-\pi^+)}{\Gamma(D^0(t) \to K^-\pi^+)}. \quad (1)$$

Hereafter, the D^0 decay time is expressed in units of τ_{D^0}, the D^0 lifetime [12], to keep the notation more compact. Expanding these ratios up to second order in the small mixing parameters x_{12} and y_{12} and, consequently, also in t, one obtains

[*]Full author list given at the end of the article.

$$R^{\pm}_{K\pi}(t) \approx R_{K\pi}(1 \pm A_{K\pi}) + \sqrt{R_{K\pi}(1 \pm A_{K\pi})}(c_{K\pi} \pm \Delta c_{K\pi})t + (c'_{K\pi} \pm \Delta c'_{K\pi})t^2, \quad (2)$$

where [13,14]

$$R_{K\pi} \equiv \frac{1}{2}\left(\left|\frac{A_{\bar{f}}}{\bar{A}_{\bar{f}}}\right|^2 + \left|\frac{\bar{A}_f}{A_f}\right|^2\right), \quad (3)$$

$$A_{K\pi} \equiv \frac{|A_{\bar{f}}/\bar{A}_{\bar{f}}|^2 - |\bar{A}_f/A_f|^2}{|A_{\bar{f}}/\bar{A}_{\bar{f}}|^2 + |\bar{A}_f/A_f|^2} \approx a^d_{\rm DCS}, \quad (4)$$

$$c_{K\pi} \approx y_{12}\cos\phi^{\Gamma}_f \cos\Delta_f + x_{12}\cos\phi^{M}_f \sin\Delta_f, \quad (5)$$

$$\Delta c_{K\pi} \approx x_{12}\sin\phi^{M}_f \cos\Delta_f - y_{12}\sin\phi^{\Gamma}_f \sin\Delta_f, \quad (6)$$

$$c'_{K\pi} \approx \frac{1}{4}(x^2_{12} + y^2_{12}), \quad (7)$$

$$\Delta c'_{K\pi} \approx \frac{1}{2}x_{12}y_{12}\sin(\phi^{M}_f - \phi^{\Gamma}_f). \quad (8)$$

Here, A_f ($\bar{A}_f$) denotes the decay amplitude of a D^0 ($\bar{D}^0$) meson into the final state $f = K^-\pi^+$; $A_{\bar{f}}$ ($\bar{A}_{\bar{f}}$) denotes the analogous amplitude for the final state $\bar{f} = K^+\pi^-$; $a^d_{\rm DCS}$ is the CP asymmetry in doubly Cabibbo-suppressed $D^0 \to K^+\pi^-$ decays; and the weak phases ϕ^M_f, ϕ^{Γ}_f, and the strong phase Δ_f are defined following the convention of Ref. [13],

$$\begin{aligned}\phi^M_f - \Delta_f &\equiv \arg(-M_{12}A_f/\bar{A}_f),\\ \phi^M_f + \Delta_f &\equiv \arg(-M_{12}A_{\bar{f}}/\bar{A}_{\bar{f}}),\\ \phi^{\Gamma}_f - \Delta_f &\equiv \arg(-\Gamma_{12}A_f/\bar{A}_f),\\ \phi^{\Gamma}_f + \Delta_f &\equiv \arg(-\Gamma_{12}A_{\bar{f}}/\bar{A}_{\bar{f}}).\end{aligned} \quad (9)$$

Finally, CP violation in Cabibbo-favored decays and relative corrections of the order of $R_{K\pi}$ are neglected in Eqs. (5)–(8). Compared to other conventions [15–18], the parametrization of Eq. (2) has the advantage of distinguishing between CP-even observables ($R_{K\pi}$, $c_{K\pi}$ and $c'_{K\pi}$) and CP-odd observables ($A_{K\pi}$, $\Delta c_{K\pi}$ and $\Delta c'_{K\pi}$), where the latter vanish in the case of no CP violation, when both ϕ^M_f and ϕ^{Γ}_f are equal to zero. Further details on different conventions and parametrizations are reported in Appendix A.

The CP asymmetry $A_{K\pi}$ provides a rigorous null test of the SM. Since the $c \to ud\bar{s}$ transition does not receive contributions from electroweak-loop (penguin) or chromomagnetic-dipole operators, any signs of CP asymmetry in the decay larger than 10^{-5} would provide unambiguous evidence of new interactions [19,20]. The same argument applies to the Cabibbo-favored $D^0 \to K^-\pi^+$ decays, where the assumption of negligible CP asymmetry is made since the contribution from the SM amplitude is much larger than that of doubly Cabibbo-suppressed $D^0 \to K^+\pi^-$ decays. The parameters $c_{K\pi}$ and, with lesser sensitivity, $c'_{K\pi}$ constrain the values of the mixing parameters x_{12} and y_{12} as well as the phase Δ_f. This phase is zero in the limit of $SU(3)_F$ flavor symmetry. Direct determinations of Δ_f at $e^+e^- \to \psi(3770)$ charm factories are available [21,22] but more precise measurements would be desirable. An indirect determination, which includes these measurements as well as LHCb measurements of the angle γ of the CKM unitarity triangle [23–25] and of charm mixing [17,26–29], achieved the best precision, yielding $\Delta_f = (-10.2 \pm 2.8)°$ [30,31]. Given the large uncertainty on the small value of Δ_f, and the level of precision with which the mixing parameters are known, $x_{12} = (4.0 \pm 0.5) \times 10^{-3}$ and $y_{12} = (6.36 \pm 0.20) \times 10^{-3}$ [31], an improved determination of $c_{K\pi}$ would mostly improve the precision on the phase Δ_f. This would improve the knowledge of $SU(3)_{\rm F}$ breaking and of rescattering at the energy scale of the charm mass [32–37], which currently limits predictions of the size of CP violation in $D^0 \to K^+K^-$ and $D^0 \to \pi^+\pi^-$ decays [38–45]. Measurements of $R_{K\pi}$, which in the $SU(3)_{\rm F}$ limit equals $|V^*_{cd}V_{us}/V^*_{cs}V_{ud}|^2 \approx (\tan\theta_{\rm C})^4$, where $\theta_{\rm C}$ is the Cabibbo angle, can also provide better insights on the size of $SU(3)_{\rm F}$ breaking. Moreover, the $D^0 \to K^+\pi^-$ and $D^0 \to K^-\pi^+$ decays are a simpler system than $D^0 \to K^+K^-$ and $D^0 \to \pi^+\pi^-$ for these studies because the distinct final-state hadrons cannot rescatter into one another. Finally, since the contribution from CP violation in decay is expected to be negligible in the SM, the parameters $\Delta c_{K\pi}$ and, again with more limited sensitivity, $\Delta c'_{K\pi}$ provide a clean measurement of CP violation in the D^0 mixing amplitudes. In fact, the phases ϕ^M_f and ϕ^{Γ}_f differ from the intrinsic mixing phases of charm mixing, ϕ^M_2 and ϕ^{Γ}_2, by $\mathcal{O}(10^{-6})$ rad (see Secs. IV B and IV C 2 of Ref. [13]). While CP violation in charm decays has been observed in $\Delta C = 1$ amplitudes [46,47], all searches for CP violation in the mixing amplitudes to date have yielded null results [17,27,28,48–50]. The small value of Δ_f, along with the similar sizes of x_{12} and y_{12}, implies better sensitivity to ϕ^M_f than to ϕ^{Γ}_f.

This article presents a measurement of $R^{\pm}_{K\pi}(t)$ performed with proton-proton (pp) collision data collected by the LHCb experiment at a center-of-mass energy of 13 TeV from 2015 through 2018, corresponding to an integrated luminosity of 6 fb^{-1}. The D^0 meson is required to originate from strong $D^*(2010)^+ \to D^0\pi^+_{\rm s}$ decays, such that its flavor at production is determined by the charge of the low-momentum "soft" pion, $\pi^+_{\rm s}$. Hereafter the $D^*(2010)^+$ meson is referred to as D^{*+}. The decay $D^0(t) \to K^+\pi^-$ is referred to as wrong sign (WS), as the charge of the pion is opposite to that of the soft pion from the D^{*+} decay, while the decay $D^0(t) \to K^-\pi^+$ is referred to as right sign (RS).

The results supersede those of a previous measurement based on the subset of data collected during 2015 and 2016 [18]. The results are finally combined with those of Run 1, also taken from Ref. [18].

II. MEASUREMENT OVERVIEW

This section introduces the methodology used in the analysis, with detailed information provided in the following sections. The analysis strategy has been revisited and improved in all aspects compared to that of Ref. [18], which used the data sample collected during the LHC Run 1 (2011–2012) and the first two years (2015–2016) of the LHC Run 2 data-taking period. The measurement described in this article extends the analysis to the full Run 2 data sample by adding data collected during 2017 and 2018, with a reanalysis of 2015 and 2016 data. The size of the full Run 2 data sample is a factor of three larger than the partial Run 2 dataset used in the previous analysis.

Signal candidates are reconstructed relying on the $D^{*+} \to D^0(\to K^{\pm}\pi^{\mp})\pi_s^+$ decay chain. Since the D^0 and π_s^+ mesons are produced with nearly collinear momenta in the laboratory frame, the resolution of the D^{*+} decay-vertex position along its momentum direction is comparable with the average D^0 flight distance, approximately 1 cm, inducing a poor decay-time resolution. The latter improves on average to about 400 μm if a kinematic fit [51] is performed requiring the D^0 meson to originate from the primary pp collision vertex (PV), exploiting the fact that most D^{*+} mesons are produced at the PV and decay strongly with negligible flight distance. This corresponds to an uncertainty on the measured D^0 decay time of about $0.1\tau_{D^0}$. This constraint also improves the D^{*+} invariant-mass resolution by a factor of two.

The dataset is divided into disjoint subsamples referred to as bins. The division is determined by the D^0 final state ($K^+\pi^-$ and $K^-\pi^+$), data-taking period (2015–2018) and D^0 decay time. In particular, there are 18 decay-time intervals in the range $[0.4, 8.0]\,\tau_{D^0}$, chosen to be equally populated except for the last four bins, which have half the number of candidates as the other bins. The raw WS-to-RS yield ratios and the average D^0 decay time and the average of its square are determined in each subsample by discriminating the signal from the background thanks to the distinctive shape of each component in the D^{*+} invariant-mass distribution. Both the RS and WS signal decays have an approximately Gaussian distribution for the D^{*+} invariant mass, with a standard deviation of approximately 0.3 MeV$/c^2$. The main background, referred to as combinatorial, consists of correctly reconstructed D^0 decays associated with an unrelated pion from the same pp collision. Another background, referred to as ghost, arises from ghost soft pions. These are fake tracks generated by combining a track stub in the vertex detector with another track stub produced by a different particle in the tracking stations downstream of the magnet (see next section for additional information on the detector layout).

The raw determinations of WS-to-RS ratios in each subsample, and for different D^0 final states, $K^+\pi^-$ and $K^-\pi^+$, are corrected for the known sources of possible bias. The most relevant ones are the contamination of doubly misidentified D^0 decays, and the removal of common candidates from the sample of WS decays. Doubly misidentified D^0 decays are proper RS decays which are misreconstructed as WS decays, where a genuine kaon is misidentified as a pion and vice-versa. The common candidates are, instead, WS D^{*-} candidates where the same D^0 candidate is also used to reconstruct a RS D^{*+} candidate with an invariant mass within 0.9 MeV$/c^2$ (approximately three times the mass resolution) from the known D^{*+} mass value [12]. The WS D^{*+} candidate is discarded since the RS D^{*-} candidate has a much higher probability of being genuine due to the much larger production rate and purity. This requirement also removes a small fraction of proper WS decays, potentially biasing the determination of the WS-to-RS ratio in each time bin.

The measured ratios are biased by instrumental charge asymmetries which shift the true ratio values of the different final states ($K^+\pi^-$ and $K^-\pi^+$) in opposite directions, mimicking a CP-violating effect. The residual instrumental asymmetry, A^I, that affects the measurement mainly originates from the combined effect of the soft-pion detection asymmetry and from the different probability of producing D^{*+} and D^{*-} mesons in the pp collisions. The detection efficiency of the kaon-pion pair instead cancels out in the ratio at first order, thanks to the removal of kinematic regions of the soft-pion phase space with very high charge asymmetry. The instrumental asymmetry is determined with high precision on data, by using an abundant calibration sample of promptly produced $D^{*+} \to D^0\pi^+$ decays, where the D^0 decays into a pair of charged kaons.

A small fraction of candidates originates from the decays of long-lived b hadrons (secondary decays), biasing the decay-time determination toward higher values. This bias is determined and corrected by exploiting simulated samples appropriately tuned to the data, and data samples where it is possible to isolate pure secondary D^{*+} decays. Other minor sources of decay-time biases are also considered and appropriately handled, such as biases on the measurement of the flight distance of the D^0 meson, and biases due to the misassociation of the D^0 meson to the correct reconstructed PV.

The expected time-dependent behavior is fitted to the measured ratios and average decay times to measure mixing and CP-violation parameters. The fit function includes the bias sources and contributions from other systematic uncertainties with constraints applied via nuisance parameters. The best-fit values of the parameters of interest were examined only after the analysis strategy was

finalized, to avoid experimenter bias. The robustness and reliability of the analysis methodology are extensively tested looking for possible unexpected variations of the measured parameters as a function of different observables related to the kinematics and topology of the decay or different conditions of the detector, suitably chosen to be sensitive to the main sources of systematic uncertainties.

III. LHCb DETECTOR

The LHCb detector [52,53] is a single-arm forward spectrometer covering the pseudorapidity range $2 < \eta < 5$, designed for the study of particles containing b or c quarks. The detector includes a high-precision tracking system consisting of a silicon-strip vertex detector surrounding the pp interaction region, a large-area silicon-strip detector located upstream of a dipole magnet with a bending power of about 4 Tm, and three stations of silicon-strip detectors and straw drift tubes placed downstream of the magnet. The tracking system provides a measurement of the momentum, p, of charged particles with a relative uncertainty that varies from 0.5% at low momentum to 1.0% at 200 GeV/c. The minimum distance of a track to a PV, the impact parameter (IP), is measured with a resolution of $(15 + 29/p_{\mathrm{T}})$ μm, where p_{T} is the component of the momentum transverse to the beam, in GeV/c. The magnetic field deflects oppositely charged particles in opposite directions, which can lead to detection asymmetries. Therefore, its polarity is reversed around every two weeks throughout the data taking to reduce such effects. Different types of charged hadrons are distinguished using information from two ring-imaging Cherenkov (RICH) detectors. Photons, electrons and hadrons are identified by a calorimeter system consisting of scintillating-pad and preshower detectors, an electromagnetic and a hadronic calorimeter. Muons are identified by a system composed of alternating layers of iron and multiwire proportional chambers.

The online event selection is performed by a trigger, which consists of a hardware stage followed by a two-level software stage, which applies a full event reconstruction. At the hardware-trigger stage, events are required to contain a muon with high p_{T} or a hadron, photon or electron with high transverse energy deposited in the calorimeters. For hadrons, the transverse energy threshold is approximately 3.7 GeV. In between the two software stages, an alignment and calibration of the detector are performed in near real-time [54] and updated constants are made available for the trigger, ensuring high-quality tracking and particle identification (PID) information. The excellent performance of the online reconstruction offers the opportunity to perform physics analyses directly using candidates reconstructed at the trigger level [55,56], which the present analysis exploits. The storage of only the triggered candidates enables a reduction in the event size by an order of magnitude.

Simulation is used to estimate the size of the bias in the measurement of the D^0 decay time, as described in Sec. VII C. In the simulation, pp collisions are generated using PYTHIA [57,58] with a specific LHCb configuration [58]. Decays of unstable particles are described by EvtGen [59], in which final-state radiation is generated using PHOTOS [60]. The interaction of the generated particles with the detector, and its response, are implemented using the Geant4 toolkit [61,62] as described in Ref. [62]. In order to increase the speed of producing simulated events and allow much larger samples to be saved on disk, the simulation of a single specific decay process can be enabled, neglecting all other particles emerging from the pp collisions. More details on the treatment of these samples are given in Sec. VII C.

IV. CANDIDATE SELECTION

The $D^{*+} \to D^0\,\pi_{\mathrm{s}}^+$ decay, where the D^0 meson decays into the $K^+\pi^-$ or $K^-\pi^+$ final state, is fully reconstructed online and selected by a dedicated trigger. The hardware trigger requires large transverse energy deposited in the calorimeters by one or both of the D^0 decay products or, alternatively, the hardware-trigger decision can be independent of the D^0 decay products and the soft pion. This requirement discards candidates selected because of the energy deposit of the soft pion and avoids the introduction of additional detection charge asymmetries. At least one (or both) of the tracks from the D^0 decay must meet the selection criteria of the single-track (two-track) first-stage software trigger. The former requires the presence of at least one track with high p_{T} and high IP significance with respect to all PVs. The latter requires that two high-p_{T} tracks form a good-quality vertex that is significantly displaced from its associated PV, defined as the PV to which the IP significance of the two-track combination is the smallest. This selection is based on a boosted decision tree classifier [63] that takes as inputs the χ^2 of the two-track vertex fit, the number of tracks with high IP significance with respect to the PV (p-value$<3.3\times10^{-4}$), the sum of the p_{T} of the two tracks, and the significance of the flight distance of their combination from the associated PV. The second-stage software trigger combines high-quality tracks with opposite charges and a distance of closest approach smaller than 0.1 mm into D^0 candidates. Each track is required to have $p > 5$ GeV/c, $p_{\mathrm{T}} > 800$ MeV/c and is assigned a pion or kaon mass hypothesis based on information from the RICH detectors. The D^0 decay vertex is required to be significantly displaced from the PV, and the angle between the D^0 momentum and the vector connecting the PV and the D^0 decay vertex is required to be less than one degree. The p_{T} of the D^0 meson is also required to be higher than 1 GeV/c. Finally, all high-quality tracks in the event that form a good-quality

vertex with the D^0 candidate, are identified as soft pions and are used to form D^{*+} candidates.

In the offline selection, π_s^+ candidates are required not to be identified as electrons or kaons by the RICH detectors and calorimeters, and are required to satisfy $p_T(\pi_s^+) > 200$ MeV/c and $\eta(\pi_s^+) < 4.3$ to reduce the combinatorial background from random associations of D^0 mesons with unrelated tracks. The requirement on the pseudorapidity also reduces detection charge asymmetries due to material interactions in the conical beampipe of the RICH detector placed after the vertex detector. The $m(D^0\pi_s^+)$ observable is the D^{*+} invariant mass measured by fixing the D^0 mass to its known value [12] when evaluating the D^{*+} candidate energy, in order to reduce the contribution from the D^0 invariant-mass resolution.

Whenever multiple D^{*+} candidates are formed using the same D^0 candidate and different soft pions with the same charge, these D^{*+} candidates are discarded, since half or more of them are background. This happens in around 9% of WS candidates. In addition, whenever a WS candidate is reconstructed also as a RS candidate, and the $m(D^0\pi_s^+)$ value of the RS candidate lies within ± 0.9 MeV/c^2 of the known D^{*+} mass [12], the WS candidate is discarded since it is likely to be either combinatorial or ghost background. This requirement rejects around 16% of the WS sample. About 40% of the residual ghost background is removed based on the output of a multivariate classifier trained using information from all tracking subdetectors to differentiate between genuine and fake tracks [64]. The soft pion is also required to satisfy the following condition, where momenta are expressed in MeV/c

$$\begin{aligned}[|p_y/p_z| > 0.015 \text{ OR } |p_x| < (470 - 0.01397 \cdot p_z) \\ \text{OR } |p_x| > (430 + 0.01605 \cdot p_z)] \\ \text{AND } [|p_x| < 0.317 \cdot (p - 2000)],\end{aligned} \quad (10)$$

where p_x, p_y, and p_z are the components of the soft-pion momentum projected onto the LHCb coordinate system.[1] This requirement rejects about 15% of the signal candidates and an additional 20% of the ghost background while also removing candidates prone to large detector asymmetries, as shown in Fig. 1. This approach closely follows that used in other LHCb precision measurements [46,47], and ensures precise and robust cancellation of instrumental charge asymmetries in the WS-to-RS yield ratios, as described in Sec. VII B. The residual background from D^0 decays with a single misidentified decay product is further strongly reduced by requiring the D^0 invariant mass,

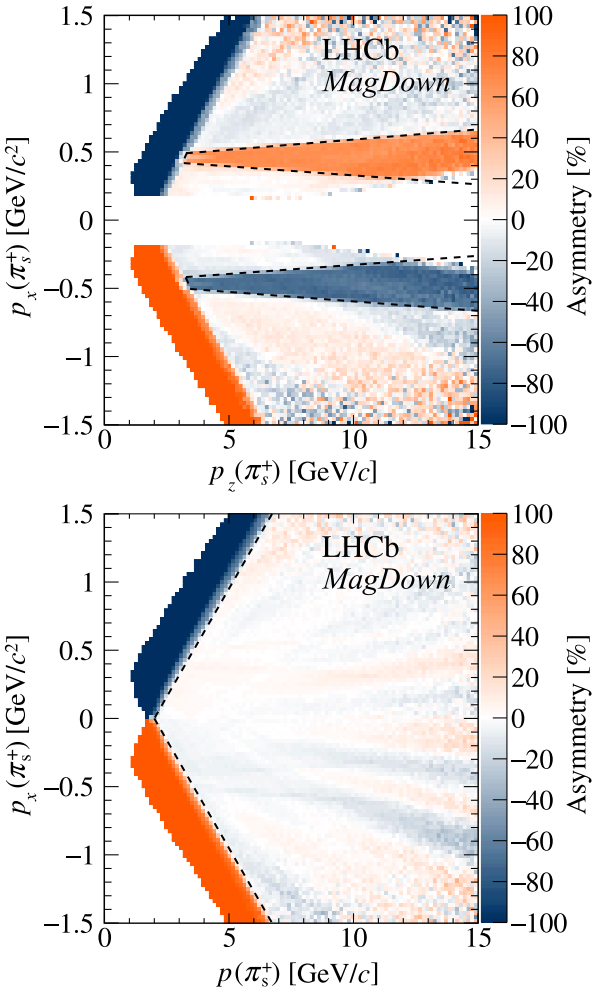

FIG. 1. Raw asymmetries of the soft pion for the RS signal candidates, with the polarity of the magnet pointing towards the negative direction of the y axis (*MagDown*). Dashed lines show the excluded regions of high detection asymmetries. The top plot includes only candidates with $|p_y/p_z| < 0.015$, i.e. the kinematic region close to the beam pipe. The bottom plot shows all candidates, except those excluded by the beam-pipe fiducial requirements.

$m(K\pi)$, to be within ± 24 MeV/c^2 of the D^0 mass [12], corresponding to around three times the mass resolution. The background from D^0 decays where the mass assignment of both the decay products is inverted is reduced by computing the D^0 invariant mass with swapped kaon-pion mass hypotheses, $m(K\pi)_{\text{swap}}$, and requiring it to be more than 16 MeV/c^2 away from the D^0 mass. This requirement removes about 11% of the signal sample while rejecting 80% of the doubly misidentified background. Secondary D^{*+} decays, unlike promptly produced decays, do not always point back to the PV. Their fraction is reduced to a few percent by requiring IP(D^0) < 60 μm.

The $m(D^0\pi_s^+)$ distributions of WS and RS candidates after all selections are shown in Fig. 2. The result of a fit to the $m(D^0\pi_s^+)$ distribution of the whole data sample is

[1]The LHCb coordinate system is a right-handed system centered on the nominal pp collision point, with the z axis pointing along the beam direction toward the detectors downstream, the y axis pointing vertically upwards, and the x axis pointing in the horizontal direction.

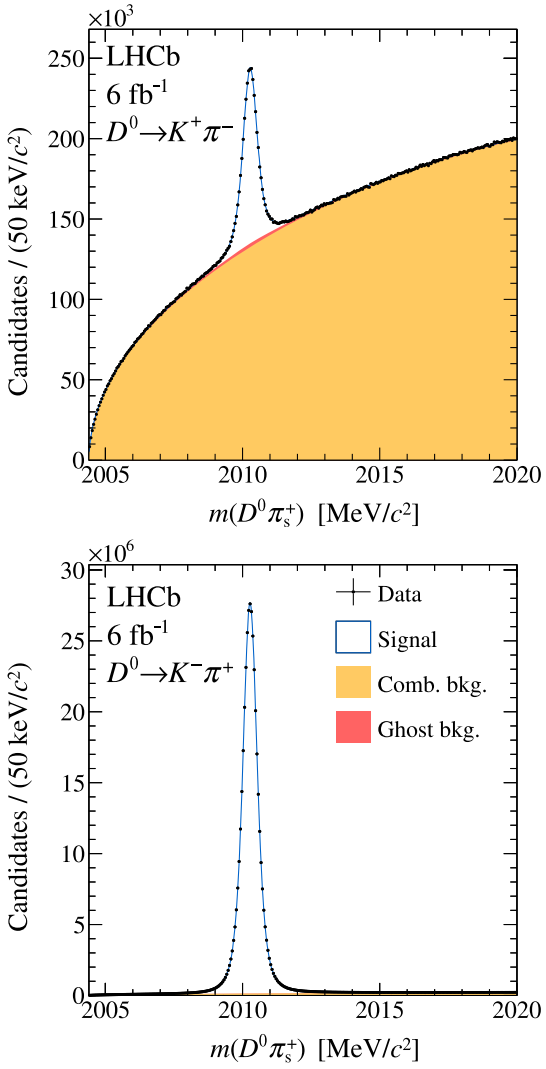

FIG. 2. Mass distribution of (top) WS and (bottom) RS candidates after the offline selection. Different fit components are displayed stacked. The ghost background component is present in both WS and RS samples, but is barely visible only in the WS one.

superimposed. The probability density functions (PDFs) employed in the fit are described in Sec. VI. Signal decays are distributed according to an approximately Gaussian PDF in the D^{*+} invariant mass with a standard deviation of about 0.3 MeV/c^2. The background is dominated by real D^0 mesons associated with uncorrelated particles and has a square-root-like shape. The small contribution from the ghost soft-pion background accounts for about 3.7% of the whole WS sample and will be discussed and quantified in the next two sections. Selecting a mass range within ± 0.6 MeV/c^2 (about two standard deviations) from the known D^{*+} mass, purities of about 99.1% and 30.9% are found for the RS and WS candidates, respectively. The signal yield is 1.6 million for WS decays and 412 million for RS decays.

V. GHOST BACKGROUND SAMPLE

As described in Sec. IV, whenever a D^0 candidate is used to reconstruct both a WS D^{*-} and a RS D^{*+} candidate, and the $m(D^0\pi_s^+)$ value of the RS candidate lies in the vicinity of the known D^{*+} mass [12], the WS candidate is discarded. The RS candidates belonging to this sample are mostly genuine D^{*+} signal decays, while the corresponding WS candidates arise from the association of the D^0 meson with a ghost soft pion or with an uncorrelated particle (in most cases, a pion originating from the PV). The opening angle between the directions of the soft pions of the WS and RS candidates, $\theta(\pi_s^+, \pi_s^-)$, allows these two different sources of backgrounds to be disentangled, as shown in the top panel of Fig. 3. The distribution of the pairs where one of the two soft pions is a ghost has a narrow peak close to zero since they share the same clusters of hits in the vertex detector. The component due to the uncorrelated particles, instead, has a much wider distribution, populating higher angle values. The requirement $\theta(\pi_s^+, \pi_s^-) < 1$ mrad selects a pure sample of

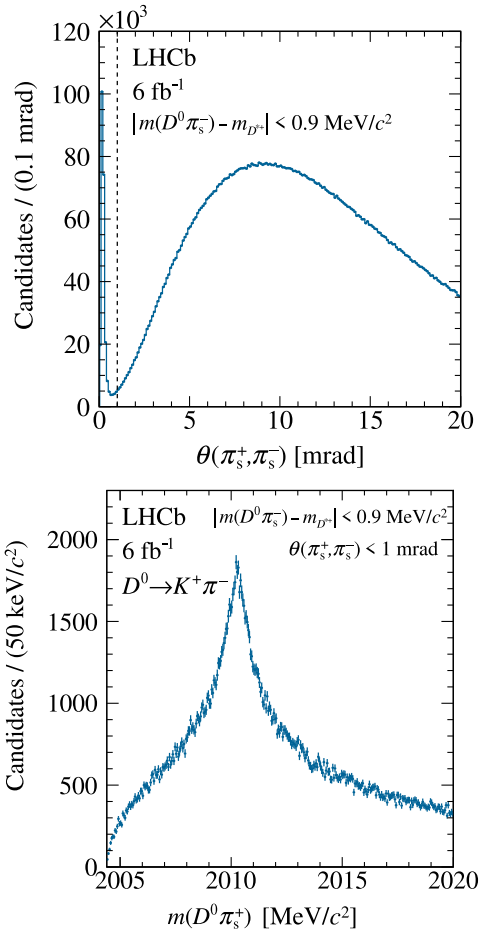

FIG. 3. Distribution of the angle between common WS and RS soft pions, $\theta(\pi_s^+, \pi_s^-)$, for the common candidates subsample (top). The 1 mrad threshold, utilized to select the common ghost candidates, is marked by a vertical dashed line. Distribution of $m(D^0\pi_s^+)$ for the common ghost candidates (bottom).

WS candidates associated with a ghost soft pion, referred to in the following as *common ghost* (CG) candidates, and their $m(D^0\pi_s^+)$ distribution is shown in the bottom panel of Fig. 3. The CG candidates are used in the analysis as a proxy for the residual ghost candidates present in the final WS (and RS) data sample. The CG candidates and the residual ghost candidates share the same features, except that they lie in two different kinematic regions of the reconstructed soft pion. The CG candidates populate regions where both the genuine RS candidate and the ghost WS candidate are reconstructed within the acceptance of the tracking stations located downstream of the magnet. The contamination of residual ghost soft pions in the signal sample, however, is mainly spatially distributed at the borders of the geometric acceptance, populating regions of the soft-pion kinematics with high charge asymmetries where, while the genuine associated RS candidate is not reconstructed, the ghost WS candidate is. Hence, this residual background of ghost candidates is highly reduced by the fiducial requirement of Eq. (10), which removes kinematic regions with large charge asymmetries in reconstructing low-momentum particles.

The features of both CG candidates and the residual ghost candidates present under the WS (and RS) signal peaks are approximately reproduced by employing a data-driven technique [65]. By selecting a pair of genuine RS candidates in data with reconstructed clusters of hits in the vertex detector very close in space, an artificial sample of ghost candidates is generated by recomputing the $m(D^0\pi_s^+)$ invariant mass of one of the two RS candidates using the momentum magnitude of the soft pion of the other one. This is repeated both for a pair of RS D^{*+} candidates within the acceptance of the final selection, passing the fiducial requirement of Eq. (10), and for a second pair of genuine RS candidates where only one candidate falls in the fiducial region. The distributions of the $m(D^0\pi_s^+)$ invariant mass for the two artificial samples are found to be compatible, validating the usage of the CG candidates as a proxy for the residual ghost background in the sample. Compatibility is also assessed between the $m(D^0\pi_s^+)$ distribution of these artificial samples and that of the CG sample, apart from a small smearing that is needed because the directions of the two-track segments in the vertex detector do not exactly coincide.

A complementary requirement on the angle, $\theta(\pi_s^+, \pi_s^-) > 1$ mrad, selects a high-purity sample of WS candidates associated with unrelated particles. This is a sample of pure combinatorial background and is used to check the reliability of the empirical function used to model this type of background component.

VI. RATIO AND AVERAGE DECAY-TIME DETERMINATION

The raw WS-to-RS yield ratios, r_i^+ and r_i^- for the $K^+\pi^-$ and $K^-\pi^+$ final states, respectively, and for each subsample i, are determined via a simultaneous χ^2 fit to the D^{*+} invariant mass, $m(D^0\pi_s^+)$, of WS, RS and CG candidates using empirical PDFs for the signal, combinatorial and ghost background shapes. While the distribution of WS and RS candidates receives contributions from these three components, that of CG candidates is only described by the ghost background shape. All parameters describing the PDFs are determined independently in each time interval from the mass fit, unless explicitly stated otherwise.

The PDFs of both WS and RS signal are modeled as the product of two functions, which together describe the distribution of the sum of promptly produced and secondary D^{*+} decays. The first one is the convolution of a Lorentz function with the sum of two Johnson S_U functions [66], while the second function serves to enforce the kinematical threshold of the D^{*+} decay, and it is equal to

$$H(m(D^0\pi_s^+) - m_0) \times (m(D^0\pi_s^+) - m_0)^\rho, \qquad (11)$$

where H is the Heaviside step function and m_0 and ρ are free parameters. The parameter m_0 is approximately equal to the sum of the D^0 and the π^+ masses. The signal shape is constrained to be the same for the WS and RS candidates in each bin, except for a global shift to the mean that takes into account small inaccuracies in the calibration of the momenta of particles of opposite charge.

The PDF of the combinatorial background, both for WS and RS candidates, is proportional to

$$\sqrt{m(D^0\pi_s^+) - m_0} \times [1 + \alpha(m(D^0\pi_s^+) - m_0) + \beta(m(D^0\pi_s^+) - m_0)^2], \qquad (12)$$

where α and β are small free parameters accounting for the deviation from a pure square-root behavior, and the m_0 parameter is shared with that of the WS and RS signal mass shapes. The PDFs of WS and RS combinatorial backgrounds have the same functional shape, but employ two different sets of parameters to account for very small contamination from misreconstructed decays of charmed mesons that may differ between RS and WS samples, but display a similar square-root behavior.

The ghost background shape is empirical and is described by the weighted sum of a Johnson S_U function and a uniform distribution, multiplied by a term that enforces the kinematic threshold, as done for the WS and RS signal PDFs. Data-driven studies of this background guarantee the reliability of some simplifying assumptions [65], which are made to ensure the convergence of the fits. The shape parameters of this component are required to be the same for the WS, RS and CG candidates, and most of them are fixed to the result of a fit to the time-integrated sample. The shape of the ghost background candidates is found to depend only weakly on the D^0 decay time, as precisely verified by comparing the

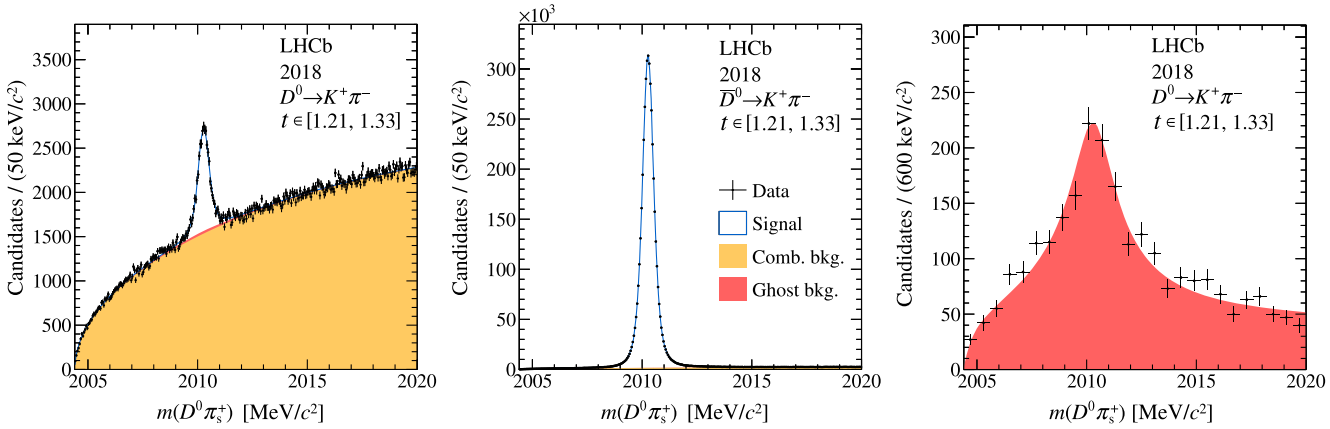

FIG. 4. An example of the $m(D^0\pi_s^+)$ distributions of (left) WS, (center) RS, (right) and CG events of the 2018 $K^+\pi^-$ sample in the $t \in [1.21, 1.33]$ decay-time interval. The value of the χ^2 per number of degrees of freedom of this fit is 653/631. Different fit components are superimposed as indicated in the legend.

distribution of CG candidates among different decay-time intervals. Moreover, the absolute number of ghost candidates is constrained to be equal in WS and RS candidates, since they are mainly generated by the same random source. This latter assumption is checked by repeating the mass fits with and without the constraint and no significant change in the final results is observed. This is expected because the fraction of ghost soft pions in the RS sample is negligible; however, this constraint is kept to improve the stability and the reproducibility of the mass fits.

Figure 4 shows the projections of a typical simultaneous fit, in a given decay-time interval, to the $m(D^0\pi_s^+)$ invariant-mass distribution of the RS, WS, and CG candidates. For RS and WS decays, different contributions from signal, combinatorial background, and CG decays are also displayed. The distribution of the measured values of the χ^2 per number of degrees of freedom (χ^2/ndf) of all 108 mass fits is found to display a Gaussian-like shape to a good approximation. The mean value is about 1.06, while its standard deviation equals about 0.07, to be compared with the expected values of 1 and 0.06, respectively. An inflation factor of $\sqrt{1.06}$ is applied to the measured uncertainties of the WS-to-RS signal ratios to account for possible small effects of the mismodeling of the empirical PDFs used. Furthermore, many checks and studies are performed on both the reliability and robustness of the adopted strategy for the fit to the D^{*+} invariant-mass distribution [65].

The average values of the decay time and of the squared decay time, $\langle t \rangle_i$ and $\langle t^2 \rangle_i$, respectively, are evaluated in each subsample i using data after removing the contribution of the combinatorial background by means of a sideband-subtraction procedure in the $m(D^0\pi_s^+)$ distribution. Background candidates in a lateral mass window, $m(D^0\pi_s^+) \in [2014, 2020]$ MeV/c^2, are weighted with a suitable negative coefficient, while candidates in the signal region, $m(D^0\pi_s^+) \in [2009.37, 2011.17]$ MeV/c^2, are left unchanged with weights equal to unity. The negative coefficient is defined as the ratio of the integral over the signal region to that over the lateral mass window of the combinatorial background PDF. The analytical model of this PDF is is determined by a mass fit similar to the one described above. Here, the constraint that the D^{*+} candidate originates from the PV is not used in the vertex fit, to include all secondary decays, which otherwise would be artificially migrated to lower masses. The ghost background component is negligible and therefore not taken into account in the fit. Uncertainties on $\langle t \rangle_i$ and $\langle t^2 \rangle_i$ are very small compared with other uncertainties on decay-time biases and are therefore neglected.

VII. SOURCES OF BIASES

A. Ratio bias

Measurements described in Refs. [18,49], using a dataset largely overlapping with that used in this analysis, precisely quantified the contamination from singly misidentified two-body decays ($D^0 \to K^+K^-$ and $D^0 \to \pi^+\pi^-$) and misreconstructed multibody charm decays, in both RS and WS data samples. From these studies, it can be concluded that these backgrounds are negligible. The main background to the RS sample is given by $D^0 \to K^-\ell^+\nu_\ell$ decays, at a level of 0.03% of the RS signal yield. The main background to the WS sample is given instead by $D^0 \to \pi^+\pi^-\pi^0$ decays at a level of about 0.1% of the WS signal yield. However, this contribution has a wider distribution in $m(D^0\pi_s^+)$, so that its contamination to the signal is further reduced when the fit to the invariant mass is performed. No evidence of CP violation has been found in dedicated studies of this decay [67–69], and it can be safely neglected.

The residual contamination from doubly misidentified $D^0 \to K^-\pi^+$ decays can mimic a time-dependent effect since it is correlated with the momentum of the D^0 meson. It is estimated via a fit to the two-dimensional distribution

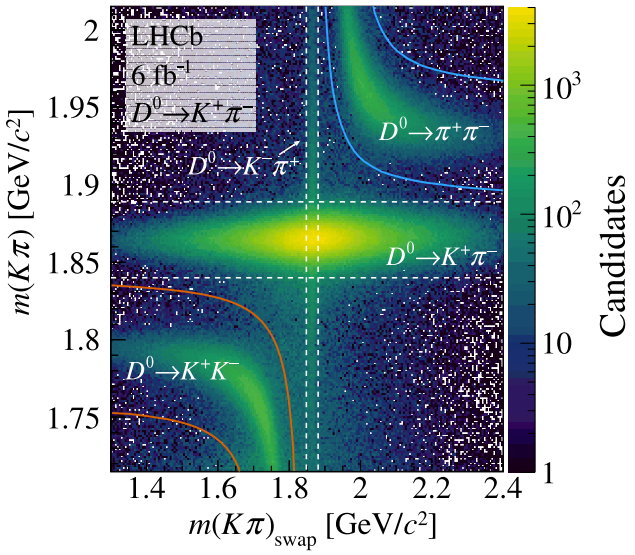

FIG. 5. Background-subtracted two-dimensional distribution of the invariant $K\,\pi$ mass, computed with the standard mass hypothesis, $m(K\pi)$, vs the swapped mass hypothesis, $m(K\pi)_{\rm swap}$, for WS candidates. Horizontal (vertical) dashed lines indicate the signal (vetoed) region, while blue (orange) solid lines indicate the region where the reconstructed invariant D^0 mass is within ± 40 MeV/c^2 of its known value when computed with the $\pi\,\pi$ ($K\,K$) mass hypothesis.

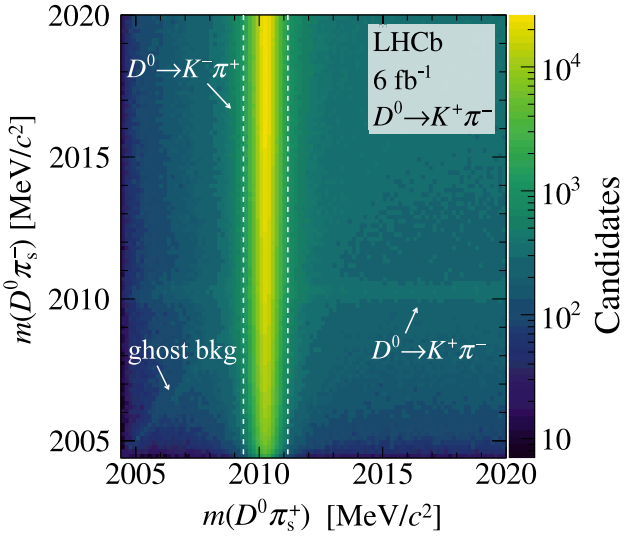

FIG. 6. Two-dimensional distribution of the invariant masses of the D^{*+} and D^{*-} mesons reconstructed from the same D^0 meson, but using two different candidates for the soft pion. Candidates in the region within the vertical dashed lines are discarded from the WS sample, as described in Sec. IV. The barely visible diagonal band is due to ghost soft pions.

of the $K\,\pi$ invariant mass computed with the correct and the inverted $K\,-\pi$ mass hypotheses, $m(K\pi)$ vs $m(K\pi)_{\rm swap}$, of background-subtracted WS candidates, where any requirement on the D^0 mass is removed, as shown in Fig. 5. After applying the requirements on both D^0 masses, the bias to the measured ratio is estimated to be 2×10^{-6} and is subtracted (see Sec. VIII). A conservative uncertainty equal to half the bias value is assigned. Time-dependent variations of this bias are smaller and are, therefore, neglected.

The fraction of signal WS decays removed by vetoing the RS and WS common candidates is determined by fitting the two-dimensional distribution of the invariant masses of the common D^{*+} and D^{*-} candidates reconstructed from the same D^0 meson, but with oppositely charged soft pions, which is shown in Fig. 6. The measured fraction is about 0.13% and the corresponding bias is subtracted (see Sec. VIII). A conservative uncertainty equal to half the bias value is again assigned, and the time-dependent variations are neglected.

B. Asymmetry bias

Nuisance charge asymmetries mainly originate from the different probabilities of producing D^{*+} and D^{*-} mesons in a pp collision and from the different efficiencies of detecting positively and negatively charged low-momentum particles, such as the soft pion utilized to form the D^{*+} candidates. The LHCb detector is not perfectly left-right symmetric, and the detection and reconstruction process, including pattern recognition, track reconstruction, and selections, is intrinsically charge-asymmetric. The net effect of such instrumental asymmetries is a bias to the WS-to-RS yield ratio, acting in opposite directions for the $K^+\pi^-$ and $K^-\pi^+$ final states, and mimicking a CP-violating asymmetry indistinguishable from a real effect due to the effective Hamiltonian for D^0 mesons. Any such asymmetry must be precisely removed.

For a given subsample i, the measured biased value of the WS-to-RS yield ratio, $\tilde{R}_i^{\pm}$, is related to the unbiased value, $R_i^{\pm}$, through the following expression

$$\tilde{R}_i^{\pm} = R_i^{\pm}(1 \pm 2A_i^{\rm I}), \tag{13}$$

where $A_i^{\rm I}$ is the instrumental asymmetry. This asymmetry is measured using a pure calibration sample of 40 million $D^{*+}\to D^0(\to K^+K^-)\pi_s^+$ decays, collected in the same conditions and with almost identical requirements as the RS and WS data samples. The raw asymmetry, a_i^{KK}, is measured from data in each subsample i by counting the number of reconstructed $D^0\to K^+K^-$ ($\bar{D}^0\to K^+K^-$) candidates, N_i^+ (N_i^-), as $a_i^{KK}=(N_i^+-N_i^-)/(N_i^++N_i^-)$. The instrumental asymmetry is determined as

$$A_i^{\rm I} = a_i^{KK} - (a_{KK}^d + \Delta Y\langle t\rangle_i). \tag{14}$$

The terms a_{KK}^d and ΔY are the CP-violating asymmetry in the decay and the time-dependent CP asymmetry in the singly Cabibbo-suppressed $D^0\to K^+K^-$ mode, respectively. They are both external inputs to this analysis and

their measured values [47,49], with the associated uncertainties, are used as nuisance parameters in the fit to the time-dependent WS-to-RS yield ratios. The average value of the decay time, in each sub-sample, is approximately equal to that of RS candidates, and is denoted by $\langle t \rangle_i$. The derivation of Eqs. (13) and (14), reported in Ref. [65], assumes small values of both production and detection asymmetries, including those of the soft pion, over the whole kinematic domain. This is enforced by the fiducial requirement on the soft-pion momentum given in Eq. (10), which allows also neglecting higher-order terms proportional to the detection asymmetry of the $K\pi$ pair.

The numbers of D^0 and $\bar{D}^0$ to K^+K^- decays in each subsample are determined by means of a simultaneous binned χ^2 fit to the $m(D^0\pi_s^+)$ invariant-mass distribution of the D^{*+} and D^{*-} candidates, which employs the same PDFs as in Sec. VI for the signal and the combinatorial background, but neglects the ghost background. The $m(D^0\pi_s^+)$ distributions of D^0 and $\bar{D}^0$ candidates after all selections are shown in Fig. 7, with the result of a fit superimposed. The quality of the fits is inspected in each subsample and no sign of mismodeling is found. The raw asymmetries are found to be stable across all data-taking periods and do not show significant decay-time dependency, as shown in Fig. 8.

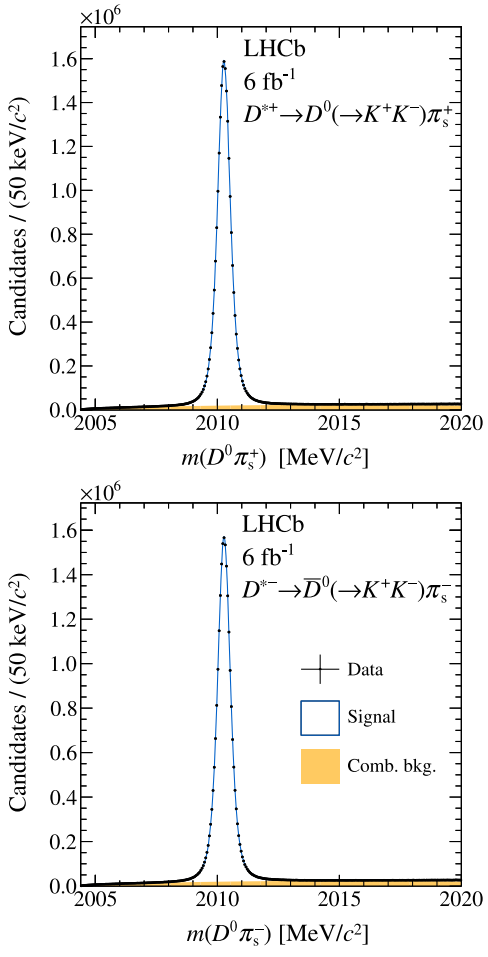

FIG. 7. Mass distributions of (top) $D^0 \to K^+K^-$ and (bottom) $\bar{D}^0 \to K^+K^-$ candidates after the offline selection, with results of the fit described in the text superimposed.

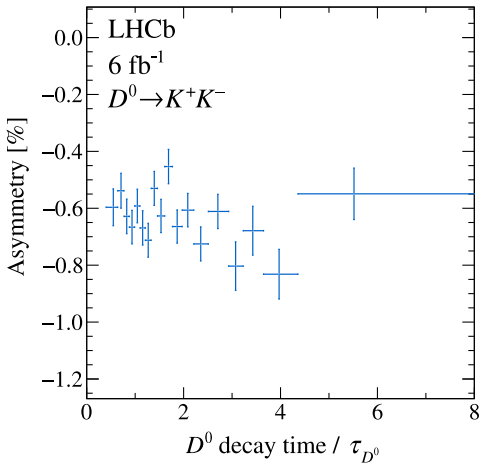

FIG. 8. Measured values of the raw asymmetry, a_i^{KK}, in each decay-time interval, for the $D^0 \to K^+K^-$ decays. Results are averaged over the different data-taking periods.

In order to measure instrumental asymmetries, A_i^{I}, in identical conditions as for RS and WS decays, a weighting procedure is applied, separately for each data-taking period and D^0 decay-time interval, to equalize the kinematics of $D^0 \to K^+K^-$ decays to that of $D^0 \to K^-\pi^+$ decays. Weights are computed by comparing the six-dimensional $(p_{\mathrm{T}}(D^0),\ \eta(D^0),\ \phi(D^0),\ p_{\mathrm{T}}(\pi_s^+),\ \eta(\pi_s^+),\ \phi(\pi_s^+))$ background-subtracted distributions between the two samples, where ϕ is the azimuthal angle with respect to the x axis. The weights are distributed close to unity since the kinematics of the two samples are very similar.

C. Decay-time bias

The contamination from secondary decays is the main source of bias to the D^0 decay-time determination. Requirements on observables sensitive to decay-time resolution at trigger level and bin migration are minor sources of decay-time bias which also affect promptly produced D^{*+} decays, hereafter called prompt decays. The total biases affecting the measured values of $\langle t \rangle$ and $\langle t^2 \rangle$, in each subsample i, are equal to

$$\langle \delta t \rangle_i = \langle \delta t \rangle_i^{\mathrm{P}}(1 - f_i) + \langle \delta t \rangle_i^{\mathrm{S}} f_i, \tag{15}$$

$$\langle \delta t^2 \rangle_i = \langle \delta t^2 \rangle_i^{\mathrm{P}}(1 - f_i) + \langle \delta t^2 \rangle_i^{\mathrm{S}} f_i, \tag{16}$$

where the superscripts P and S indicate that the average is that for prompt and secondary decays, respectively, and f_i is the fraction of secondary decays in each bin i. The values of $\langle \delta t \rangle_i$ and $\langle \delta t^2 \rangle_i$ for prompt and secondary candidates and

the relative fraction f_i, for each data-taking period are determined by performing a template fit to the two-dimensional IP(D^0) vs t distribution of the background-subtracted RS candidates, where $K^+\pi^-$ and $K^-\pi^+$ final states are combined. The discriminating power in disentangling the prompt and secondary component is increased by loosening the requirement on the IP of the D^0 meson to IP(D^0) < 600 μm. This also allows checking that the distribution of the secondary decays, which mostly populate regions with high values of the IP, is accurately modeled.

The two-dimensional templates are generated with a Geant4 -based simulation which simulates only prompt and secondary D^{*+} decays, neglecting all other particles emerging from the pp collisions. The detector resolutions and efficiencies evaluated in these samples are expected to be superior to those of the full simulation due to the considerably lower detector occupancy. However, this approach increases the speed of producing simulated events by approximately a factor of 50, and allows much larger samples of events to be saved on disk, with no trigger and offline requirements applied except those related to the LHCb geometrical acceptance. Thus, the detector response can be accurately tuned to match data in relevant variables such as the vertex resolution. The absence of the underlying event emerging from pp collisions causes loss of information on the reconstructed PV position. This is addressed by smearing the true PV position of each simulated event according to the covariance matrix obtained from the PV fit in data, properly reproducing the behavior observed in data, including tails and dependence on track and vertex multiplicities. To improve the level of agreement between data and simulation, the resolution of the D^0 decay vertex (DV) in simulation is weighted to be on average the same as that of data. Moreover, a misalignment of about 10 μm is observed in data between the left and right halves of the vertex detector, which broadens the IP(D^0) distributions. Since the size of this effect is not accurately reproduced in simulated samples, a misalignment of the same size is applied to match data. Smaller simulated samples with the underlying event emerging from the pp collisions are also available and are used to check all aspects of the analysis related to the full topology of the event, such as the probability of associating an incorrect PV to the D^{*+} candidate.

The kinematics of the simulated D^0 mesons and soft pions are weighted in the multidimensional space of their momenta to align with data [70]. The weights are computed using data sets with IP(D^0) < 60 μm (> 120 μm) for prompt (secondary) decay candidates. The first subsample coincides with the signal sample, enriched with prompt decays. The contribution of the small residual contamination of secondaries, which is the target of this study, does not affect the momentum distributions and it is, therefore, neglected for the purpose of weighing the simulated samples. The latter subsample is a pure sample of secondary decays.

The sample of simulated secondary decays accounts for all known b hadrons decaying into a generic final state with a D^{*+} meson. Production fractions of different hadrons and branching fractions of all the considered decay modes are taken from Ref. [12]. To account for the limited knowledge of the composition of this sample, a small number of $B^0 \to D^{*+}X$ decays, where X is a particle of arbitrary mass, is simulated and added to the mixture. Both the relative fraction, f_X, of this decay mode and the mass, m_X, of the X particle are treated as nuisance parameters in the template fit. This is intended to be an effective correction, as confirmed by the small size of observed discrepancies. In support of this approach, a satisfactory level of compatibility between data and simulation is found when the D^{*+} meson is required to form a good vertex with a charged muon. This is a very pure sample of $\bar{B}^0 \to D^{*+}\mu^-\bar{\nu}_\mu$ decays, and it can be directly compared with simulated decays without any contamination from unknown decay modes and external inputs.

Systematic uncertainties from the limited knowledge of the PV and DV resolution, f_X and m_X are treated with the template profile likelihood approach [71]. Templates are produced with the PV and DV resolution independently scaled by a factor of 0.9, 1 and 1.1 of the baseline scenario, f_X is chosen equal to 0%, 3% and 6%, m_X is chosen between 0.5, 1.5 and 2.5 GeV/c^2. Templates corresponding to intermediate values of these nuisance parameters are obtained through piece-wise linear interpolation. Uncertainties on the number of events in the bins of the templates are treated using the Beeston–Barlow prescription [72]. The only free parameters in the fit relate to the normalization of the prompt and secondary templates, and the four nuisance parameters described above. The fitted values for the PV (DV) resolution scale factors are within 1.07–1.09 (1.02–1.04), while a relative fraction of about 1% is found for an effective particle with mass $m_X \approx 0.8 - 1.3$ GeV/c^2. Prompt and secondary simulated samples are then used to determine the biases $\langle \delta t^{(2)} \rangle_i^P$, $\langle \delta t^{(2)} \rangle_i^S$, and the relative fraction f_i in each subsample i. The agreement between data and fit projections is shown in Fig. 9. The main discrepancies are attributed to the simulation accuracy in replicating trigger requirements at low decay times. They are accounted for, both in the estimation of the relative fractions f_i and of decay-time biases, by inflating uncertainties by a factor of $\sqrt{\chi^2/\mathrm{ndf}}$, separately for each decay-time bin. These discrepancies affect prompt and secondary decays similarly, and to a substantial extent cancel out in the computation of f_i fractions. The measured values of the total bias $\langle \delta t \rangle_i$, with the separate contributions from prompt and secondary decays, are shown in Fig. 10, together with the measured relative fractions, f_i, of secondary decays. The uncertainties on the $\langle \delta t \rangle_i$ parameters are also determined from the simulated samples of prompt and secondary decays, and

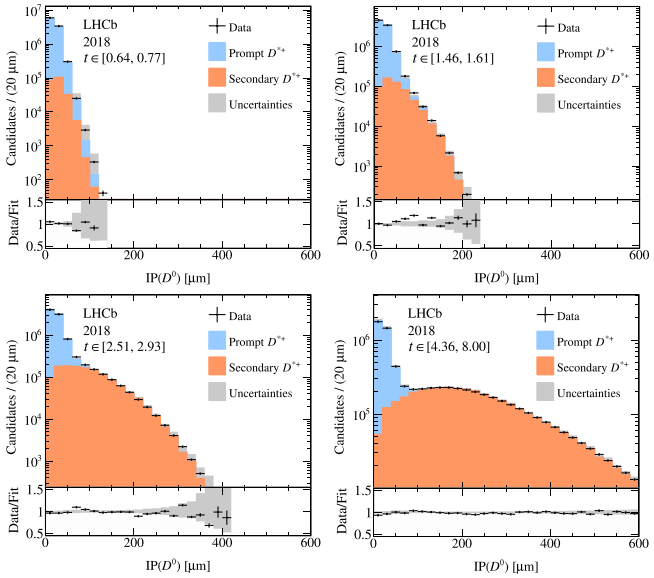

FIG. 9. Distributions of the IP of the RS sample candidates from the 2018 data-taking period for different decay-time intervals. The projections of the two-dimensional template fit are superimposed. The points in the lower panel of each plot show the data-to-fit ratio, where the vertical black lines represent the statistical uncertainties of data, and the grey error band displays the total uncertainty of the simulation.

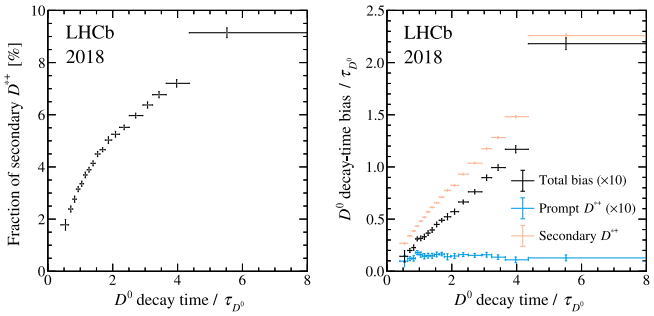

FIG. 10. Relative fraction of D^{*+} candidates from b hadrons as a function of the D^0 decay time (left). Total decay-time bias as a function of the D^0 decay time (right). Values of the decay-time bias for the prompt and secondary components are also shown. The D^{*+} candidates are required to have IP(D^0) less than 60 μm.

include both statistical and systematic contributions. These uncertainties are correlated and the associated covariance matrix is used in the fit of the oscillation parameters, described in the next section.

VIII. DETERMINATION OF OSCILLATION PARAMETERS

The decay-time dependence of the WS-to-RS ratio is fitted to the observed ratios, simultaneously for the two D^0 final states, to determine the mixing and CP-violation parameters. In the following, the uncertainties of measured quantities are indicated by σ. The minimized χ^2 is

$$\chi^2 = \sum_{j,y,f} \left(\frac{r^f_{jy} - R^f_{jy}}{\epsilon \sigma(r^f_{jy})} \right)^2 + \chi^2_{\text{nuis}}, \tag{17}$$

where the sum spans over all the 18 decay-time intervals, j, three data-taking periods, y, and the two D^0 final states, $f \in \{+, -\}$. The terms r^f_{jy} are the measured raw ratios, while their associated uncertainties are indicated with $\sigma(r^f_{jy})$. Small generic mismodeling found in the D^{*+} mass fits is accounted by an uncertainty inflation factor, $\epsilon = \sqrt{1.06}$, chosen such that the average reduced χ^2 of the fits to the D^{*+} mass is equal to unity as explained in Sec. VI. The expected WS-to-RS ratios, $R^{\pm}_{jy}$, are written accounting for corrections as

$$\begin{aligned} R^{\pm}_{jy} \equiv [&R_{K\pi}(1 \pm A_{K\pi}) \\ &+ \sqrt{R_{K\pi}(1 \pm A_{K\pi})}(c_{K\pi} \pm \Delta c_{K\pi})\langle T \rangle^{\pm}_{jy} \\ &+ (c'_{K\pi} \pm \Delta c'_{K\pi})\langle T^2 \rangle^{\pm}_{jy}] \\ &\times (1 \pm 2A^{\pm}_{jy} - C) + D, \end{aligned} \tag{18}$$

where $R_{K\pi}$, $c_{K\pi}$, $c'_{K\pi}$, $A_{K\pi}$, $\Delta c_{K\pi}$ and $\Delta c'_{K\pi}$ are the six parameters of interest. The terms $\langle T^{(2)} \rangle^{\pm}_{jy}$ are the corrected average values of the (squared) decay time, defined as

$$\langle T^{(2)} \rangle^{\pm}_{jy} \equiv (\langle t^{(2)} \rangle^{\pm}_{jy} - \langle \delta T^{(2)} \rangle_{jy}) \cdot S^{(2)}, \tag{19}$$

where $\langle t^{(2)} \rangle^{\pm}_{jy}$ are the measured average (squared) decay times and the terms $\delta \langle T^{(2)} \rangle_{jy}$ are the nuisance fit parameters associated to the measured biases of the decay time. The scale factor parameter S accounts for the uncertainty of the m_{D^0}/τ_{D^0} ratio. The A_{jy} term in Eq. (18) is the instrumental asymmetry, defined as

$$A^{\pm}_{jy} \equiv A^{KK}_{jy} - A^{d}_{KK} - \delta y \cdot \langle T \rangle^{\pm}_{jy}, \tag{20}$$

where A^{KK}_{jy}, A^{d}_{KK} and δy are the fit nuisance parameters associated to the measured raw asymmetry of the $D^0 \to K^+K^-$ signal candidates (weighted to the RS sample), the CP asymmetry in the decay $D^0 \to K^+K^-$ and the corresponding time-dependent CP-violating asymmetry, respectively. The nuisance parameter C in Eq. (18) is the relative fraction of WS signal candidates discarded with the removal of the RS-WS common candidates, while D is the nuisance parameter that accounts for the bias caused by the residual small contamination of doubly misidentified RS candidates. Nuisance parameters are constrained to be within uncertainties of their measured values by the term

$$\chi^2_{\text{nuis}} = \sum_{y,i,j}(\delta\theta^i_y - \delta\Theta^i_y)[\text{Cov}^{-1}_y(\delta\theta)]^{ij}(\delta\theta^j_y - \delta\Theta^j_y) + \left(\frac{s-S}{\sigma(s)}\right)^2 + \left(\frac{c-C}{\sigma(c)}\right)^2 + \left(\frac{d-D}{\sigma(d)}\right)^2 + \sum_{t,y}\left(\frac{a^{KK}_{jy} - A^{KK}_{jy}}{\sigma(a^{KK}_{jy})}\right)^2 + \left(\frac{a^d_{KK} - A^d_{KK}}{\sigma(a^d_{KK})}\right)^2 + \left(\frac{\Delta Y - \delta y}{\sigma(\Delta Y)}\right)^2, \quad (21)$$

where $\delta\theta_y$ and $\text{Cov}_y(\delta\theta)$ are the measured vectors of decay-time biases for different data-taking periods, defined as $\delta\theta_y \equiv [\langle\delta t\rangle_{1y}, \langle\delta t^2\rangle_{1y}, \langle\delta t\rangle_{2y}, \langle\delta t^2\rangle_{2y}, \cdots]$, and their covariance matrices, respectively, while $\delta\Theta$ is the vector of nuisance fit parameters associated to the determined bias values of the decay time, similarly defined as $\delta\Theta_y \equiv [\langle\delta T\rangle_{1y}, \langle\delta T^2\rangle_{1y}, \langle\delta T\rangle_{2y}, \langle\delta T^2\rangle_{2y}, \cdots]$. The term a^{KK}_{jy} is the measured raw asymmetry in the $D^0 \to K^+K^-$ signal candidates, c is the measured fraction of WS signal candidates discarded with the removal of the RS-WS common candidates, and d is the measured bias caused by the residual contamination from doubly misidentified RS candidates. The values and associated uncertainties of the external inputs a^d_{KK}, ΔY, m_{D^0}, τ_{D^0} are taken from Refs. [12,73]: $a^d_{KK} = (4.5 \pm 5.3) \times 10^{-4}$, $\Delta Y = (-0.89 \pm 1.13) \times 10^{-4}$, $m_{D^0} = 1864.84 \pm 0.05$ MeV/c^2 and $\tau_{D^0} = 410.3 \pm 1.0$ fs. Finally, the value of s is 1.0 and its uncertainty is determined as $\sigma^2(s) = \sigma^2(m_{D^0})/m^2_{D^0} + \sigma^2(\tau_{D^0})/\tau^2_{D^0}$.

The world average values of the external inputs a^d_{KK} and ΔY are largely dominated by the LHCb Run 2 measurements of the time-integrated and the time-dependent CP violation in $D^0 \to K^+K^-$ decays [47,49], which mostly share the same candidates used for correcting the nuisance charge asymmetries in this measurement. However, the statistical correlation of mixing and CP-violation observables with a^d_{KK} and ΔY is small and is neglected in Eq. (17). The statistical uncertainty of the a^d_{KK} measurement is dominated by the size of the $D^+ \to K^0_S\pi^+$ and $D^+_s \to K^0_S K^+$ calibration samples, used to precisely remove production and detection asymmetries [47], while the measurement of $A_{K\pi}$ reported in this article is largely dominated by that of the WS data sample. This results in a correlation of about 1% between $A_{K\pi}$ and the two individual measurements of the time-integrated CP violation in the $D^0 \to K^+K^-$ decays of Ref. [47]. The correlation of $\Delta c_{K\pi}$ and $\Delta c'_{K\pi}$ with the measurement of ΔY [49] is about 3%, and its impact is completely negligible as also shown in Table II. For similar reasons a correlation of about 30% between the LHCb measurements of a^d_{KK} and ΔY observables is also neglected in the minimization of the χ^2 reported in Eq. (17). An alternative fit, where the observables are slightly modified to be independent of these external inputs, such that the results can be directly used in global fits to the charm mixing and CP-violation parameters [31,73], is described in Appendix B. This alternative configuration also has the advantage that it can be used, under the assumption of negligible CP violation in doubly Cabibbo-suppressed decays, to measure a^d_{KK} with improved precision.

To search for undetected systematic uncertainties, the analysis is repeated on statistically independent data subsets chosen to be sensitive to specific sources of bias. These criteria include the data-taking year (2015–2018), the magnetic field orientation, the number of primary vertices in the event, the trigger category, the soft-pion momentum, the kinematic region of the soft pions (inside and on the border of the geometrical acceptance), and the output of the multivariate classifier used to remove ghost soft pions. The resulting variations of the measured parameters are consistent with statistical fluctuations, with p-values in the 9%–86% range. The stability of the results over the data-taking periods, trigger categories, and detector occupancy confirms the robustness of the analysis methodologies against any change due to different running and data-acquisition conditions, and aging of the LHCb detector over the years. The compatibility of the results obtained by repeating the whole measurement for candidates collected with the two different magnet polarities probes the robustness and reliability of the corrections for the instrumental asymmetries. The consistency of the results in these two samples is considered a powerful validation of the analysis method, since without the application of the corrections a significant inconsistency is seen. The stability of the results as a function of the soft-pion momentum, and therefore as a function of the D^0 momentum, probes any subtle unknown effect due to track reconstruction algorithms, as well as any impact of the residual contamination from doubly misidentified RS candidates. Finally, repeating the measurement in different kinematic regions of the soft pions and in different intervals of the output of the multivariate classifier used to remove ghost soft-pion candidates is of paramount importance to ensure that removal of the ghost candidates is accurate and within the assessed uncertainties.

IX. RESULTS AND SYSTEMATIC UNCERTAINTIES

The fit results are presented in Table I, where the uncertainties include both statistical and systematic contributions. An ensemble of pseudoexperiments confirms that the extracted parameters are without perceivable bias and that the size of the parameter correlations are within expectations. Fit projections, averaged over the three data-taking periods, are reported in Fig. 11. The obtained p-value of the fit is 0.91 (0.84), when the inflation factor ϵ is considered (not considered). The fit is repeated in the scenario where CP violation is not allowed, by requiring

TABLE I. Results of the fit to the time dependence of the WS-to-RS ratio. Uncertainties and correlations include both statistical and systematic contributions.

Parameters		Correlations [%]				
		$c_{K\pi}$	$c'_{K\pi}$	$A_{K\pi}$	$\Delta c_{K\pi}$	$\Delta c'_{K\pi}$
$R_{K\pi}$	$(343.1 \pm 2.0) \times 10^{-5}$	−92.4	80.0	0.9	−0.8	0.1
$c_{K\pi}$	$(51.4 \pm 3.5) \times 10^{-4}$		−94.1	−1.4	1.4	−0.7
$c'_{K\pi}$	$(13.1 \pm 3.7) \times 10^{-6}$			0.7	−0.7	0.1
$A_{K\pi}$	$(-7.1 \pm 6.0) \times 10^{-3}$				−91.5	79.4
$\Delta c_{K\pi}$	$(3.0 \pm 3.6) \times 10^{-4}$					−94.1
$\Delta c'_{K\pi}$	$(-1.9 \pm 3.8) \times 10^{-6}$					

$A_{K\pi} = 0$, $\Delta c_{K\pi} = 0$ and $\Delta c'_{K\pi} = 0$. The consistency of the data with the hypothesis of CP symmetry is determined from the change in χ^2 between the fits assuming CP conservation and allowing for CP violation. The results are compatible with the hypothesis of CP symmetry with a p-value of 0.57. The significance of the quadratic term in the decay-time-dependent ratio is similarly evaluated by repeating the fit with and without fixing $c'_{K\pi}$ to zero. The difference in the χ^2 value gives a significance of 3.4 standard deviations against the hypothesis of $c'_{K\pi} = 0$. This is the first measurement to have significant sensitivity to the quadratic term. The systematic uncertainties are summarized in Table II, where the contribution from each source is obtained by repeating the fit with the associated nuisance parameters fixed to their best-fit values and subtracting the resulting covariance matrix from the one of the unconstrained fit. The "mass modeling" contribution accounts for possible imperfections of the used empirical PDFs and is determined by repeating the fit by fixing the inflation factor ϵ to 1. The "ghost soft pions" contribution quantifies the impact on the analysis of the uncertainty on this component, and is determined by repeating all $m(D^0\pi_s^+)$ mass fits fixing the parameters of the PDF of the ghost component, in each decay-time interval, to those obtained in the baseline fits where they are free to float. The "instrumental asymmetry" contribution refers to the uncertainties on the nuisance parameters A_{jy}^{KK}, which account for the statistical uncertainties in measuring the raw asymmetry in the $D^0 \to K^+K^-$ signal candidates, and is relevant only for the CP-violation parameters. The contributions from "a_{KK}^d input" and "ΔY input" account for the uncertainties of the world-average values of these observables. The contributions "doubly misID" and "common candidates" refer to the uncertainty related to the estimate of the bias caused by the doubly misidentified RS candidates and to the uncertainty on the relative fraction of discarded WS candidates due to the removal of common WS-RS candidates. They are determined by repeating the fit with the nuisance parameters C and D, respectively, fixed to their best-fit values. The item "decay-time bias" accounts for the uncertainties in the determination of the decay-time biases, which include biases from trigger-induced effects, uncertainties in the PV and DV resolutions, misalignments in the vertex detector, the composition of the simulated sample of secondary D^{*+} decays, the finite size of the simulation sample, and inflation of the uncertainty to account for local disagreements in the template fit. The systematic uncertainty is determined by repeating the fit while fixing the values of the $\langle \delta t \rangle_{jy}$ terms to their best-fit values. The last

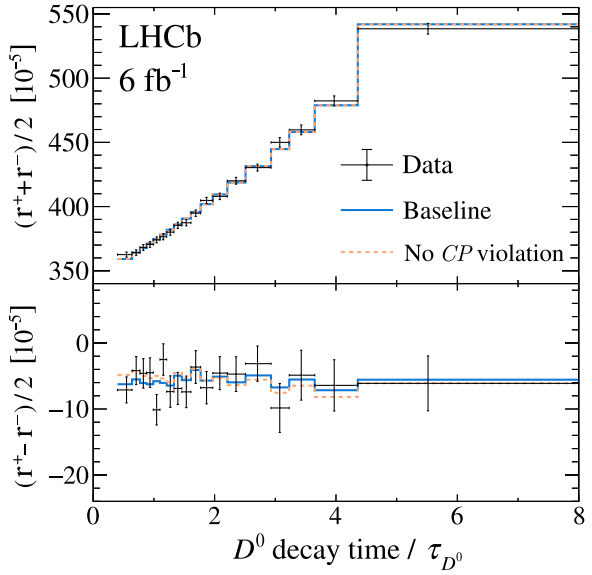

FIG. 11. Half sum and half difference of measured WS-to-RS yields ratio for the $K^+\pi^-$ and $K^-\pi^+$ final states as a function of decay time. Projections of fits where CP -violation effects are allowed (solid line) or forbidden (dotted line) are overlaid. The abscissa of each data point corresponds to the average decay time over the bin, the horizontal error bars delimit the bin, and the vertical error bars indicate the statistical uncertainties.

TABLE II. Summary of the statistical (stat.) and systematic (syst.) uncertainties (unc.). Dots are used to indicate values below 0.1 in the relevant units for that column. The abbreviations "Instr." and "cand." stand for "Instrumental" and "candidates", respectively.

Source	$R_{K\pi}$ [10^{-5}]	$c_{K\pi}$ [10^{-4}]	$c'_{K\pi}$ [10^{-6}]	$A_{K\pi}$ [10^{-3}]	$\Delta c_{K\pi}$ [10^{-4}]	$\Delta c'_{K\pi}$ [10^{-6}]
Mass modeling	0.5	0.8	0.9	1.4	0.8	0.8
Ghost soft pions	0.4	0.8	0.8	1.1	0.8	1.1
Instr. asymmetry	...	...	...	1.2	0.7	0.7
a_{KK}^d input	...	...	...	1.1	...	...
ΔY input	...	...	...	...	0.1	0.1
Doubly misID	0.1	0.1	0.1	...	...	...
Common cand.	0.2	...	...	...	...	...
Decay-time bias	0.1	0.2	0.1	0.1	...	...
m_{D^0}/τ_{D^0} input	...	0.1	0.1	...	...	...
Total syst. unc.	0.7	1.1	1.2	2.4	1.3	1.4
Stat. unc.	1.9	3.3	3.5	5.5	3.3	3.5
Total unc.	2.0	3.5	3.7	6.0	3.6	3.8

TABLE III. Results of the combination of the measurements using Run 1 and Run 2 data. Uncertainties and correlations include both statistical and systematic contributions.

Parameters		Correlations [%]				
		$c_{K\pi}$	$c'_{K\pi}$	$A_{K\pi}$	$\Delta c_{K\pi}$	$\Delta c'_{K\pi}$
$R_{K\pi}$	$(342.7 \pm 1.9) \times 10^{-5}$	−92.7	80.3	0.9	−0.7	0.2
$c_{K\pi}$	$(52.8 \pm 3.3) \times 10^{-4}$		−94.2	−1.3	1.2	−0.7
$c'_{K\pi}$	$(12.0 \pm 3.5) \times 10^{-6}$			0.7	−0.7	0.2
$A_{K\pi}$	$(-6.6 \pm 5.7) \times 10^{-3}$				−91.9	79.7
$\Delta c_{K\pi}$	$(2.0 \pm 3.4) \times 10^{-4}$					−94.1
$\Delta c'_{K\pi}$	$(-0.7 \pm 3.6) \times 10^{-6}$					

contribution in the table refers to the scale factor s, which accounts for the uncertainty on the knowledge of the m_{D^0}/τ_{D^0} ratio. The leading systematic uncertainties are those associated with the D^{*+} mass fit and the modeling of the ghost background; the results are dominated by statistical uncertainties.

The results presented in this article extend and supersede the measurement of mixing and CP-violation parameters with promptly produced $D^0 \to K^+\pi^-$ decays published in Ref. [18] to the full LHC Run 2 data sample, by adding data collected during 2017 and 2018, and by reanalyzing data collected in 2015 and 2016 with improved methodologies. The analysis of Ref. [18] used data collected during LHC Run 1 (2011–2012) combined with those from 2015 and 2016. Since the 2015 and 2016 samples are used in both this analysis and the previous one, and separate results for Run 1 and 2 data were not presented in Ref. [18], the measurements cannot be combined naively. Furthermore, the results reported in Ref. [74], based on Run 1 data alone, cannot be used, since the bias due to the contamination of ghost soft pions was not accounted for at that time. To obtain results using LHCb's full available sample of prompt $D^0 \to K^+\pi^-$ decays, the measurement of the full LHC Run 2 data sample, presented in this article, is combined with the previous LHCb measurement based on the data collected during 2011 and 2012 [18], by minimizing a total $\chi^2 = \chi^2_{\text{Run1}} + \chi^2_{\text{Run2}}$, where the term χ^2_{Run2} is that described in Eq. (17), while the term χ^2_{Run1} is recomputed using internal LHCb documentation, and exactly matches the analysis of Ref. [18], including all systematic uncertainties and nuisance parameters. There are no correlations between the two measurements and the two χ^2 terms are treated as independent. The final LHCb Run 1 and Run 2 results are consistent with each other, and the combination reported in Table III improves the final uncertainties compared to Run 2 alone by about 7%.

X. CONCLUSIONS

A measurement of the time-dependent ratio of the $D^0 \to K^+\pi^-$ to $\bar{D}^0 \to K^+\pi^-$ decay rates is performed at the LHCb experiment using proton-proton collisions at a center-of-mass energy of 13 TeV, corresponding to an integrated luminosity of 6 fb^{-1}, collected from 2015 through 2018. The D^0 meson is required to originate from a prompt $D^*(2010)^+ \to D^0\pi^+$ decay, such that its flavor at production is inferred from the charge of the soft pion. The measurement is performed simultaneously for the $K^+\pi^-$ and $K^-\pi^+$ final states, allowing both mixing and CP-violation parameters to be determined. Results are averaged with those obtained from Ref. [18] employing data recorded by the LHCb experiment during 2011 and 2012 at a center-of-mass energy of 7 TeV and 8 TeV, respectively, providing the legacy LHCb Run 1 and Run 2 measurement.

The results for all measured parameters are the most precise to date, and will significantly improve the precision of the world averages [30,31,73]. The improvement factor of the total uncertainties with respect to the previous most precise set of measurements, also from LHCb [18], is in the range of 1.5–1.6 for both mixing and CP-violation parameters, in line with the increase of the data sample size due to the inclusion of 2017 and 2018 data. The most dominant source of systematic uncertainty of the previous measurement, due to the bias generated by the residual contamination of D^{*+} decays originating from a b-hadron decay, is reduced by more than one order of magnitude. On average, the reduction of the total systematic uncertainties is about a factor of two, paving the way for even better precision in future measurements with larger data samples.

The parameter $A_{K\pi}$ provides a rigorous null test of the SM by probing CP violation in the decay $D^0 \to K^+\pi^-$, and it is found to be consistent with CP symmetry within an uncertainty of 5.7×10^{-3}. The parameters $c_{K\pi}$ and $c'_{K\pi}$ constrain the values of the mixing parameters x_{12} and y_{12} and the phase Δ_f. Since the value of y_{12} is precisely known, particularly thanks to the recent measurement of the parameter $y_{CP} = y_{12}\cos\phi_2^\Gamma$ [29] in singly Cabibbo-suppressed $D^0 \to K^+K^-$ and $D^0 \to \pi^+\pi^-$ decays, the improvement in precision on $c_{K\pi}$ mainly impacts the accuracy in the determination of the strong phase Δ_f [75], once the new results are combined with other relevant measurements from the charm and beauty sector following the approach of Ref. [30]. The results [75] point to a significant departure, exceeding 4 Gaussian-equivalent standard deviations, of Δ_f from the value of zero expected in the $SU(3)_F$ symmetry limit, and they can provide insights on $SU(3)_F$ breaking and rescattering at the energy scale of the charm quark mass. The precision of the new results also allows for the first time to have significant sensitivity to the quadratic term $c'_{K\pi}$ of the time-dependent expansion, which is found to deviate from zero with a significance of 3.4 Gaussian-equivalent standard deviations. Finally, the achieved accuracy on the parameter $\Delta c_{K\pi}$ provides a clean test of CP violation in the interference between D^0 mixing and decay, and will improve the knowledge of the dispersive mixing phase ϕ_2^M by about 16% [75,76].

ACKNOWLEDGMENTS

We express our gratitude to our colleagues in the CERN accelerator departments for the excellent performance of the LHC. We thank the technical and administrative staff at the LHCb institutes. We acknowledge support from CERN and from the national agencies: CAPES, CNPq, FAPERJ and FINEP (Brazil); MOST and NSFC (China); CNRS/IN2P3 (France); BMBF, DFG and MPG (Germany); INFN (Italy); NWO (Netherlands); MNiSW and NCN (Poland); MCID/IFA (Romania); MICIU and AEI (Spain); SNSF and SER (Switzerland); NASU (Ukraine); STFC (United Kingdom); DOE NP and NSF (U.S.). We acknowledge the computing resources that are provided by CERN, IN2P3 (France), KIT and DESY (Germany), INFN (Italy), SURF (Netherlands), PIC (Spain), GridPP (United Kingdom), CSCS (Switzerland), IFIN-HH (Romania), CBPF (Brazil), and Polish WLCG (Poland). We are indebted to the communities behind the multiple open-source software packages on which we depend. Individual groups or members have received support from ARC and ARDC (Australia); Key Research Program of Frontier Sciences of CAS, CAS PIFI, CAS CCEPP, Fundamental Research Funds for the Central Universities, and Sci. & Tech. Program of Guangzhou (China); Minciencias (Colombia); EPLANET, Marie Skłodowska-Curie Actions, ERC and NextGenerationEU (European Union); A*MIDEX, ANR, IPhU and Labex P2IO, and Région Auvergne-Rhône-Alpes (France); AvH Foundation (Germany); ICSC (Italy); Severo Ochoa and María de Maeztu Units of Excellence, GVA, XuntaGal, GENCAT, InTalent-Inditex and Prog. Atracción Talento CM (Spain); SRC (Sweden); the Leverhulme Trust, the Royal Society and UKRI (United Kingdom).

APPENDIX A: ALTERNATIVE PARAMETRIZATIONS OF THE OBSERVABLES

The parametrization of Eq. (2) is trivially related to that in Eq. (73) of Ref. [13],

$$R^{\pm}_{K\pi}(t) \approx R^{\pm}_{K\pi} + \sqrt{R^{\pm}_{K\pi}}c^{\pm}_{\mathrm{WS},f}t + c'^{\pm}_{\mathrm{WS},f}t^2, \tag{A1}$$

as follows,

$$\begin{aligned}
R_{K\pi} &= \frac{R^{+}_{K\pi} + R^{-}_{K\pi}}{2},\\
A_{K\pi} &= \frac{R^{+}_{K\pi} - R^{-}_{K\pi}}{R^{+}_{K\pi} + R^{-}_{K\pi}},\\
c_{K\pi} &= \frac{c^{+}_{\mathrm{WS},f} + c^{-}_{\mathrm{WS},f}}{2},\\
\Delta c_{K\pi} &= \frac{c^{+}_{\mathrm{WS},f} - c^{-}_{\mathrm{WS},f}}{2},\\
c'_{K\pi} &= \frac{c'^{+}_{\mathrm{WS},f} + c'^{-}_{\mathrm{WS},f}}{2},\\
\Delta c'_{K\pi} &= \frac{c'^{+}_{\mathrm{WS},f} - c'^{-}_{\mathrm{WS},f}}{2}.
\end{aligned} \tag{A2}$$

The parameters $c^{\pm}_{\mathrm{WS},f}$ and $c'^{\pm}_{\mathrm{WS},f}$ are often denoted as $y'^{\pm}$ and $[(x'^{\pm})^2 + (y'^{\pm})^2]/4$, respectively. The definition of the phase Δ_f in Eq. (9) follows the convention adopted in Ref. [13], and is related to those employed in Refs. [30,31,73] as $\Delta_f = \pi - \delta_D^{K\pi} = -\delta_{K\pi}$.

In the phenomenological parametrization of CP violation, defining the two mass eigenstates of the neutral charm meson system as $|D_{1,2}\rangle \equiv p|D^0\rangle \pm q|\bar{D}^0\rangle$, with p and q complex numbers satisfying $|p|^2 + |q|^2 = 1$ (CPT invariance is assumed), and adopting the conventions that $CP|D^0\rangle = -|\bar{D}^0\rangle$ and that $|D_2\rangle$ is the CP-even eigenstate in the limit of CP symmetry in charm mixing, the mixing parameters are defined as $x \equiv (m_2 - m_1)/\Gamma$ and $y \equiv (\Gamma_2 - \Gamma_1)/2\Gamma$, and are equal to x_{12} and y_{12} up to second order in $\sin(\phi_2^M - \phi_2^\Gamma)$. Finally, adopting the following convention for the weak phase responsible for CP violation in the mixing [13],

$$\begin{aligned}
\phi_{\lambda_f} + \Delta_f &\equiv \arg\left(\frac{q\bar{A}_f}{pA_f}\right),\\
\phi_{\lambda_f} - \Delta_f &\equiv \arg\left(\frac{q\bar{A}_{\bar{f}}}{pA_{\bar{f}}}\right),
\end{aligned} \tag{A3}$$

the coefficients in Eq. (A1) can be expressed as

$$c^{\pm}_{\mathrm{WS},f} \approx \left|\frac{q}{p}\right|^{\pm 1}[y\cos(\Delta_f \mp \phi_{\lambda_f}) + x\sin(\Delta_f \mp \phi_{\lambda_f})], \tag{A4}$$

$$c'^{\pm}_{\mathrm{WS},f} \approx \frac{1}{4}(x^2 + y^2)\left|\frac{q}{p}\right|^{\pm 2}. \tag{A5}$$

Second-order corrections to the expressions above, which are negligible within the current experimental precision, can be found in Ref. [14]. The phase ϕ_{λ_f} differs from the phase ϕ_2 defined in Sec. IV B of Ref. [13], and denoted as ϕ in Refs. [30,31,73], by $O(10^{-6})$ rad, cf. Sec. IV C 2 of Ref. [13].

APPENDIX B: RESULTS WITHOUT EXTERNAL CONSTRAINTS

The time-dependent fit, described in Sec. VIII, is repeated removing the nuisance parameters A^d_{KK} and δy. The Gaussian constraints associated with the external measurement of a^d_{KK} and ΔY are consequently removed from Eq. (21). Equation (18) is modified as follows,

$$\begin{aligned}
R^{\pm}_{jy} \equiv \Big[&R_{K\pi}(1 \pm \tilde{A}_{K\pi})\\
&+ \sqrt{R_{K\pi}(1 \pm \tilde{A}_{K\pi})}(c_{K\pi} \pm \Delta\tilde{c}_{K\pi})\langle T\rangle^{\pm}_{jy}\\
&+ (c'_{K\pi} \pm \Delta\tilde{c}'_{K\pi})\langle T^2\rangle^{\pm}_{jy}\Big]\\
&\times (1 \pm 2A^{KK}_{jy} - C) + D,
\end{aligned} \tag{B1}$$

TABLE IV. Results of the combination of the measurements using Run 1 and Run 2 data without external constraints on a^d_{KK}, ΔY, and s. Uncertainties and correlations include both statistical and systematic contributions.

Parameters		Correlations [%]							
		$c_{K\pi}$	$c'_{K\pi}$	$\tilde{A}_{K\pi}$	$\Delta\tilde{c}_{K\pi}$	$\Delta\tilde{c}'_{K\pi}$	$A_{K\pi}$	$\Delta c_{K\pi}$	$\Delta c'_{K\pi}$
$R_{K\pi}$	$(342.7 \pm 1.9) \times 10^{-5}$	−92.7	80.3	0.8	−0.7	0.0	0.3	−0.2	0.2
$c_{K\pi}$	$(52.8 \pm 3.3) \times 10^{-4}$		−94.3	−1.4	1.3	−0.6	−0.5	0.4	−0.4
$c'_{K\pi}$	$(12.0 \pm 3.5) \times 10^{-6}$			0.7	−0.6	0.0	0.3	−0.3	0.3
$\tilde{A}_{K\pi}$	$(-8.2 \pm 5.9) \times 10^{-3}$				−93.4	81.0	0.0	0.0	0.0
$\Delta\tilde{c}_{K\pi}$	$(3.2 \pm 3.6) \times 10^{-4}$					−94.3	0.0	0.0	0.0
$\Delta\tilde{c}'_{K\pi}$	$(-2.0 \pm 3.8) \times 10^{-6}$						0.0	0.0	0.0
$A_{K\pi}$	$(-0.9 \pm 2.0) \times 10^{-2}$							−93.8	81.1
$\Delta c_{K\pi}$	$(-0.1 \pm 1.0) \times 10^{-3}$								−94.3
$\Delta c'_{K\pi}$	$(4.6 \pm 9.8) \times 10^{-6}$								

where the CP asymmetry of the $D^0 \to K^+K^-$ decay is absorbed into a new set of CP-violation observables, which are approximately equal to

$$\tilde{A}_{K\pi} \approx A_{K\pi} - 2a^d_{KK}, \tag{B2}$$

$$\Delta\tilde{c}_{K\pi} \approx \Delta c_{K\pi} - c_{K\pi}a^d_{KK} - 2\sqrt{R_{K\pi}}\Delta Y, \tag{B3}$$

$$\Delta\tilde{c}'_{K\pi} \approx \Delta c'_{K\pi} - 2c'_{K\pi}a^d_{KK} - 2\sqrt{R_{K\pi}}c_{K\pi}\Delta Y, \tag{B4}$$

where terms equal to $2\sqrt{R_{K\pi}} \cdot c_{K\pi} \cdot \Delta Y(\langle T^2\rangle^{\pm}_{jy} - (\langle T\rangle^{\pm}_{jy})^2)$ and to $-2c'_{K\pi}\Delta Y\langle T^2\rangle^{\pm}_{jy}\langle T\rangle^{\pm}_{jy}$ are neglected in Eq. (B1). For completeness, note that Eqs. (B3) and (B4) include terms that are of the same order as those neglected in Eqs. (5)–(8). Higher-order corrections to Eqs. (5)–(8) can be found in Ref. [14]. The measurement of $\tilde{A}_{K\pi}$ does not rely on the assumption of CP symmetry in Cabibbo-favored $D^0 \to K^-\pi^+$ decays, contrary to all previous measurements of this decay channel. The expressions for Eqs. (4)–(8), modified to account for CP violation in Cabibbo-favored decays, can be found in Ref. [14].

The combination of the present Run 2 measurement with the previous one of Run 1 from Ref. [18], described in Sec. IX, is also slightly modified to account for the different approach utilized to remove the detection charge asymmetries. The Run 1 measurement did not use any experimental information from $D^0 \to K^+K^-$ decays. Therefore, the removal of the constraints on the nuisance parameters A^d_{KK} and δy does not affect the associated χ^2_{Run1} term. Thus, the parameters $\tilde{A}_{K\pi}$, $\Delta\tilde{c}_{K\pi}$, and $\Delta\tilde{c}'_{K\pi}$ are used to probe CP violation in Run 2 data, while the parameters $A_{K\pi}$, $\Delta c_{K\pi}$, and $\Delta c'_{K\pi}$ are used in Run 1 data. The parameters $R_{K\pi}$, $c_{K\pi}$, and $c'_{K\pi}$ are unchanged and shared between the two χ^2 terms. Finally, the constraint on the parameter $s \propto m_{D^0}/\tau_{D^0}$ is also removed, and the parameter s is fixed to unity in the time-dependent fit. The impact of this constraint on the results is negligible, as the relative uncertainty on this parameter, 0.25% [12], is much smaller than that on the measurement of the other observables.

The results without external constraints on a^d_{KK} and ΔY and using this parametrization are reported in Table IV. They can be combined with other relevant measurements from the charm and beauty sector following the approach of Refs. [30,73], with and without any desired constraint [75]. For instance, this measurement acquires sensitivity to the a^d_{KK} parameter if CP symmetry is assumed in doubly Cabibbo-suppressed $D^0 \to K^+\pi^-$ decays, as expected in the SM and in many of its extensions [19,20], namely $A_{K\pi} = 0$. With this assumption, an improvement in precision of about 10% is obtained in the global fits to charm measurements for the determination of the a^d_{KK} observable [75], with a similar improvement on the corresponding observable for the $D^0 \to \pi^+\pi^-$ decay, $a^d_{\pi\pi}$, where a nonzero value with a significance exceeding 3 standard deviations has been recently found [47].

[1] S. L. Glashow, J. Iliopoulos, and L. Maiani, Weak interactions with lepton–hadron symmetry, Phys. Rev. D **2**, 1285 (1970).
[2] A. Buras, in *Gauge Theories of Weak Decays*, (Cambridge University Press, Cambridge, England, 2020), pp. 71–73, 10.1017/9781139524100.
[3] N. Cabibbo, Unitary symmetry and leptonic decays, Phys. Rev. Lett. **10**, 531 (1963).
[4] M. Kobayashi and T. Maskawa, CP-violation in the renormalizable theory of weak interaction, Prog. Theor. Phys. **49**, 652 (1973).

[5] R. K. Ellis *et al.*, Physics briefing book: Input for the European strategy for particle physics update 2020, arXiv: 1910.11775.

[6] I. Bediaga and C. Göbel, Direct *CP* violation in beauty and charm hadron decays, Prog. Part. Nucl. Phys. **114**, 103808 (2020).

[7] A. Lenz and G. Wilkinson, Mixing and *CP* violation in the charm system, Annu. Rev. Nucl. Part. Sci. **71**, 59 (2021).

[8] H. Gisbert, M. Golz, and D. S. Mitzel, Theoretical and experimental status of rare charm decays, Mod. Phys. Lett. A **36**, 2130002 (2021).

[9] T. Pajero, Recent advances in charm mixing and *CP* violation at LHCb, Mod. Phys. Lett. A **37**, 2230012 (2022).

[10] A. L. Kagan and M. D. Sokoloff, Indirect *CP* violation and implications for $D^0 - \bar{D}^0$ and $B_s^0 - \bar{B}_s^0$ mixing, Phys. Rev. D **80**, 076008 (2009).

[11] Y. Grossman, Y. Nir, and G. Perez, Testing new indirect *CP* violation, Phys. Rev. Lett. **103**, 071602 (2009).

[12] R. L. Workman *et al.* (Particle Data Group), Review of particle physics, Prog. Theor. Exp. Phys. **2022**, 083C01 (2022).

[13] A. L. Kagan and L. Silvestrini, Dispersive and absorptive *CP* violation in $D^0 - \bar{D}^0$ mixing, Phys. Rev. D **103**, 053008 (2021).

[14] T. Pajero and M. J. Morello, Mixing and *CP* violation in $D^0 \to K^-\pi^+$ decays, J. High Energy Phys. 03 (2022) 162.

[15] B. Aubert *et al.* (*BABAR* Collaboration), Evidence for $D^0 - \bar{D}^0$ mixing, Phys. Rev. Lett. **98**, 211802 (2007).

[16] B. R. Ko *et al.* (Belle Collaboration), Observation of $D^0 - \bar{D}^0$ mixing in e^+e^- collisions, Phys. Rev. Lett. **112**, 111801 (2014); **112**, 139903(E) (2014).

[17] R. Aaij *et al.* (LHCb Collaboration), Measurements of charm mixing and *CP* violation using $D^0 \to K^\pm\pi^\mp$ decays, Phys. Rev. D **95**, 052004 (2017); **96**, 099907(E) (2017).

[18] R. Aaij *et al.* (LHCb Collaboration), Updated determination of $D^0 - \bar{D}^0$ mixing and *CP* violation parameters with $D^0 \to K^+\pi^-$ decays, Phys. Rev. D **97**, 031101 (2018).

[19] S. Bergmann and Y. Nir, New physics effects in doubly Cabibbo suppressed *D* decays, J. High Energy Phys. 09 (1999) 031.

[20] Y. Grossman, A. L. Kagan, and Y. Nir, New physics and *CP* violation in singly Cabibbo suppressed D decays, Phys. Rev. D **75**, 036008 (2007).

[21] D. M. Asner *et al.* (CLEO Collaboration), Updated measurement of the strong phase in $D^0 \to K^+\pi^-$ decay using quantum correlations in $e^+e^- \to D^0\bar{D}^0$ at CLEO, Phys. Rev. D **86**, 112001 (2012).

[22] M. Ablikim *et al.* (BESIII Collaboration), Improved measurement of the strong-phase difference $\delta_D^{K\pi}$ in quantum-correlated $D\bar{D}$ decays, Eur. Phys. J. C **82**, 1009 (2022).

[23] R. Aaij *et al.* (LHCb Collaboration), Measurement of the CKM angle γ in $B^\pm \to DK^\pm$ and $B^\pm \to D\pi^\pm$ decays with $D \to K_S^0 h^+ h^-$, J. High Energy Phys. 02 (2021) 169.

[24] R. Aaij *et al.* (LHCb Collaboration), Measurement of *CP* observables in $B^\pm \to D^{(*)}K^\pm$ and $B^\pm \to D^{(*)}\pi^\pm$ decays using two-body *D* final states, J. High Energy Phys. 04 (2021) 081.

[25] R. Aaij *et al.* (LHCb Collaboration), Measurement of the CKM angle γ with $B^\mp \to D[K^\pm\pi^\mp\pi^\mp\pi^\pm]h^\mp$ decays using a binned phase-space approach, J. High Energy Phys. 07 (2023) 138.

[26] R. Aaij *et al.* (LHCb Collaboration), Measurement of the charm-mixing parameter y_{CP}, Phys. Rev. Lett. **122**, 011802 (2019).

[27] R. Aaij *et al.* (LHCb Collaboration), Measurement of the mass difference between neutral charm-meson eigenstates, Phys. Rev. Lett. **122**, 231802 (2019).

[28] R. Aaij *et al.* (LHCb Collaboration), Observation of the mass difference between neutral charm-meson eigenstates, Phys. Rev. Lett. **127**, 111801 (2021); **131**, 079901(E) (2023).

[29] R. Aaij *et al.* (LHCb Collaboration), Measurement of the charm mixing parameter $y_{CP} - y_{CP}^{K\pi}$ using two-body D^0 meson decays, Phys. Rev. D **105**, 092013 (2022).

[30] R. Aaij *et al.* (LHCb Collaboration), Simultaneous determination of CKM angle γ and charm mixing parameters, J. High Energy Phys. 12 (**2021**) 141.

[31] LHCb Collaboration, Simultaneous determination of the CKM angle γ and parameters related to mixing and *CP* violation in the charm sector, Report No. LHCb-CONF-2022-003, 2022, https://cds.cern.ch/record/2838029.

[32] L.-L. Chau and H.-Y. Cheng, SU(3) breaking effects in charmed meson decays, Phys. Lett. B **333**, 514 (1994).

[33] F. Buccella, M. Lusignoli, G. Miele, A. Pugliese, and P. Santorelli, Nonleptonic weak decays of charmed mesons, Phys. Rev. D **51**, 3478 (1995).

[34] T. E. Browder and S. Pakvasa, Experimental implications of large *CP* violation and final state interactions in the search for $D^0 - \bar{D}^0$ mixing, Phys. Lett. B **383**, 475 (1996).

[35] A. F. Falk, Y. Nir, and A. A. Petrov, Strong phases and $D^0 - \bar{D}^0$ mixing parameters, J. High Energy Phys. 12 (1999) 019.

[36] D.-N. Gao, Strong phases, asymmetries, and SU(3) symmetry breaking in $D \to K\pi$ decays, Phys. Lett. B **645**, 59 (2007).

[37] F. Buccella, A. Paul, and P. Santorelli, $SU(3)_F$ breaking through final state interactions and *CP* asymmetries in $D \to PP$ decays, Phys. Rev. D **99**, 113001 (2019).

[38] E. Franco, S. Mishima, and L. Silvestrini, The standard model confronts *CP* violation in $D^0 \to \pi^+\pi^-$ and $D^0 \to K^+K^-$, J. High Energy Phys. 05 (2012) 140.

[39] A. Khodjamirian and A. A. Petrov, Direct *CP* asymmetry in $D \to \pi^-\pi^+$ and $D \to K^-K^+$ in QCD-based approach, Phys. Lett. B **774**, 235 (2017).

[40] M. Chala, A. Lenz, A. V. Rusov, and J. Scholtz, ΔA_{CP} within the standard model and beyond, J. High Energy Phys. 07 (2019) 161.

[41] Y. Grossman and S. Schacht, The emergence of the $\Delta U = 0$ rule in charm physics, J. High Energy Phys. 07 (2019) 020.

[42] S. Schacht and A. Soni, Enhancement of charm *CP* violation due to nearby resonances, Phys. Lett. B **825**, 136855 (2022).

[43] A. Pich, E. Solomonidi, and L. Vale Silva, Final-state interactions in the *CP* asymmetries of charm-meson two-body decays, Phys. Rev. D **108**, 036026 (2023).

[44] M. Gavrilova, Y. Grossman, and S. Schacht, Determination of the $D \to \pi\pi$ ratio of penguin over tree diagrams, Phys. Rev. D **109**, 033011 (2024).

[45] A. Lenz, M. L. Piscopo, and A. V. Rusov, Two body non-leptonic D^0 decays from LCSR and implications for $\Delta a_{CP}^{\rm dir}$, J. High Energy Phys. 03 (2024) 151.

[46] R. Aaij *et al.* (LHCb Collaboration), Observation of *CP* violation in charm decays, Phys. Rev. Lett. **122**, 211803 (2019).

[47] R. Aaij *et al.* (LHCb Collaboration), Measurement of the time-integrated *CP* asymmetry in $D^0 \to K^-K^+$ decays, Phys. Rev. Lett. **131**, 091802 (2023).

[48] R. Aaij *et al.* (LHCb Collaboration), Updated measurement of decay-time-dependent *CP* asymmetries in $D^0 \to K^+K^-$ and $D^0 \to \pi^+\pi^-$ decays, Phys. Rev. D **101**, 012005 (2020).

[49] R. Aaij *et al.* (LHCb Collaboration), Search for time-dependent *CP* violation in $D^0 \to K^+K^-$ and $D^0 \to \pi^+\pi^-$ decays, Phys. Rev. D **104**, 072010 (2021).

[50] R. Aaij *et al.* (LHCb Collaboration), Model-indepedent measurement of charm mixing parameters in $\bar{B} \to D^0(\to K^{*0}\pi^+\pi^-)\mu^-\bar{\nu}_\mu X$ decays, Phys. Rev. D **108**, 052005 (2023).

[51] W. D. Hulsbergen, Decay chain fitting with a Kalman filter, Nucl. Instrum. Methods Phys. Res., Sect. A **552**, 566 (2005).

[52] A. A. Alves Jr. *et al.* (LHCb Collaboration), The LHCb detector at the LHC, J. Instrum. **3**, S08005 (2008).

[53] LHCb Collaboration, LHCb detector performance, Int. J. Mod. Phys. A **30**, 1530022 (2015).

[54] G. Dujany and B. Storaci, Real-time alignment and calibration of the LHCb detector in Run II, J. Phys. Conf. Ser. **664**, 082010 (2015).

[55] R. Aaij *et al.*, The LHCb trigger and its performance in 2011, J. Instrum. **8**, P04022 (2013).

[56] R. Aaij *et al.*, Tesla: An application for real-time data analysis in high energy physics, Comput. Phys. Commun. **208**, 35 (2016).

[57] T. Sjöstrand, S. Mrenna, and P. Skands, A brief introduction to PYTHIA 8.1, Comput. Phys. Commun. **178**, 852 (2008).T. Sjöstrand, S. Mrenna, and P. Skands, PYTHIA 6.4 physics and manual, J. High Energy Phys. 05 (2006) 026.

[58] I. Belyaev *et al.*, Handling of the generation of primary events in Gauss, the LHCb simulation framework, J. Phys. Conf. Ser. **331**, 032047 (2011).

[59] D. J. Lange, The EvtGen particle decay simulation package, Nucl. Instrum. Methods Phys. Res., Sect. A **462**, 152 (2001).

[60] N. Davidson, T. Przedzinski, and Z. Was, PHOTOS interface in C++: Technical and physics documentation, Comput. Phys. Commun. **199**, 86 (2016).

[61] J. Allison *et al.* (Geant4 Collaboration), Geant4 developments and applications, IEEE Trans. Nucl. Sci. **53**, 270 (2006); S. Agostinelli *et al.* (Geant4 Collaboration), Geant4: A simulation toolkit, Nucl. Instrum. Methods Phys. Res., Sect. A **506**, 250 (2003).

[62] M. Clemencic, G. Corti, S. Easo, C. R. Jones, S. Miglioranzi, M. Pappagallo, and P. Robbe, The LHCb simulation application, Gauss: Design, evolution and experience, J. Phys. Conf. Ser. **331**, 032023 (2011).

[63] V. V. Gligorov and M. Williams, Efficient, reliable and fast high-level triggering using a bonsai boosted decision tree, J. Instrum. **8**, P02013 (2013).

[64] M. De Cian, S. Farry, P. Seyfert, and S. Stahl, Fast neural-net based fake track rejection in the LHCb reconstruction, Report No. LHCb-PUB-2017-011, 2017, https://cds.cern.ch/record/2255039.

[65] R. Ribatti, Measurement of $D^0 - \bar{D}^0$ mixing parameters and search for *CP* violation in $D^0 \to K^+\pi^-$ decays with LHCb Run 2 data, Ph.D thesis CERN-THESIS-2024-080, Scuola Normale Superiore, 2024, https://cds.cern.ch/record/2902239.

[66] N. L. Johnson, Systems of frequency curves generated by methods of translation, Biometrika **36**, 149 (1949).

[67] R. Aaij *et al.* (LHCb Collaboration), Search for *CP* violation in the phase space of $D^0 \to \pi^+\pi^-\pi^0$ decays with the energy test, J. High Energy Phys. 09 (2023) 129.

[68] R. Aaij *et al.* (LHCb Collaboration), Search for time-dependent *CP* violation in $D^0 \to \pi^+\pi^-\pi^0$ decays, Phys. Rev. Lett. **133**, 101803 (2024).

[69] B. Aubert *et al.* (*BABAR* Collaboration), Search for *CP* violation in neutral *D* meson Cabibbo-suppressed three-body decays, Phys. Rev. D **78**, 051102 (2008).

[70] A. Rogozhnikov, Reweighting with boosted decision trees, J. Phys. Conf. Ser. **762**, 012036 (2016).

[71] K. Cranmer *et al.* (ROOT Collaboration), *HistFactory: A Tool for Creating Statistical Models for Use with RooFit and RooStats* (New York University, New York, 2012), 10.17181/CERN-OPEN-2012-016.

[72] R. J. Barlow and C. Beeston, Fitting using finite Monte Carlo samples, Comput. Phys. Commun. **77**, 219 (1993).

[73] Y. Amhis *et al.*, Averages of *b*-hadron, *c*-hadron, and τ-lepton properties as of 2021, Phys. Rev. D **107**, 052008 (2023).

[74] R. Aaij *et al.* (LHCb Collaboration), Measurement of $D^0 - \bar{D}^0$ mixing parameters and search for *CP* violation using $D^0 \to K^+\pi^-$ decays, Phys. Rev. Lett. **111**, 251801 (2013).

[75] LHCb Collaboration, Simultaneous determination of the CKM angle γ and parameters related to mixing and *CP* violation in the charm sector, Report No. LHCb-CONF-2024-004, 2024, https://cds.cern.ch/record/2905625.

[76] T. Pajero and M. J. Morello, Charm fitter, https://github.com/tpajero/charm-fitter (2022).

R. Aaij,[36] A. S. W. Abdelmotteleb,[55] C. Abellan Beteta,[49] F. Abudinén,[55] T. Ackernley,[59] A. A. Adefisoye,[67] B. Adeva,[45] M. Adinolfi,[53] P. Adlarson,[79] C. Agapopoulou,[13] C. A. Aidala,[80] Z. Ajaltouni,[11] S. Akar,[64] K. Akiba,[36] P. Albicocco,[26] J. Albrecht,[18] F. Alessio,[47] M. Alexander,[58] Z. Aliouche,[61] P. Alvarez Cartelle,[54] R. Amalric,[15] S. Amato,[3] J. L. Amey,[53] Y. Amhis,[13,47] L. An,[6] L. Anderlini,[25] M. Andersson,[49] A. Andreianov,[42] P. Andreola,[49] M. Andreotti,[24] D. Andreou,[67] A. Anelli,[29,b] D. Ao,[7] F. Archilli,[35,c]

M. Argenton,[24] S. Arguedas Cuendis,[9] A. Artamonov,[42] M. Artuso,[67] E. Aslanides,[12] R. Ataíde Da Silva,[48] M. Atzeni,[63] B. Audurier,[14] D. Bacher,[62] I. Bachiller Perea,[10] S. Bachmann,[20] M. Bachmayer,[48] J. J. Back,[55] P. Baladron Rodriguez,[45] V. Balagura,[14] W. Baldini,[24] H. Bao,[7] J. Baptista de Souza Leite,[59] M. Barbetti,[25,d] I. R. Barbosa,[68] R. J. Barlow,[61] M. Barnyakov,[23] S. Barsuk,[13] W. Barter,[57] M. Bartolini,[54] J. Bartz,[67] J. M. Basels,[16] G. Bassi,[33,e] B. Batsukh,[5] A. Bay,[48] A. Beck,[55] M. Becker,[18] F. Bedeschi,[33] I. B. Bediaga,[2] S. Belin,[45] V. Bellee,[49] K. Belous,[42] I. Belov,[27] I. Belyaev,[34] G. Benane,[12] G. Bencivenni,[26] E. Ben-Haim,[15] A. Berezhnoy,[42] R. Bernet,[49] S. Bernet Andres,[43] A. Bertolin,[31] C. Betancourt,[49] F. Betti,[57] J. Bex,[54] Ia. Bezshyiko,[49] J. Bhom,[39] M. S. Bieker,[18] N. V. Biesuz,[24] P. Billoir,[15] A. Biolchini,[36] M. Birch,[60] F. C. R. Bishop,[10] A. Bitadze,[61] A. Bizzeti, T. Blake,[55] F. Blanc,[48] J. E. Blank,[18] S. Blusk,[67] V. Bocharnikov,[42] J. A. Boelhauve,[18] O. Boente Garcia,[14] T. Boettcher,[64] A. Bohare,[57] A. Boldyrev,[42] C. S. Bolognani,[76] R. Bolzonella,[24,f] N. Bondar,[42] F. Borgato,[31,g] S. Borghi,[61] M. Borsato,[29,b] J. T. Borsuk,[39] S. A. Bouchiba,[48] T. J. V. Bowcock,[59] A. Boyer,[47] C. Bozzi,[24] A. Brea Rodriguez,[48] N. Breer,[18] J. Brodzicka,[39] A. Brossa Gonzalo,[45,55,44,a] J. Brown,[59] D. Brundu,[30] E. Buchanan,[57] A. Buonaura,[49] L. Buonincontri,[31,g] A. T. Burke,[61] C. Burr,[47] A. Butkevich,[42] J. S. Butter,[54] J. Buytaert,[47] W. Byczynski,[47] S. Cadeddu,[30] H. Cai,[72] R. Calabrese,[24,f] S. Calderon Ramirez,[9] L. Calefice,[44] S. Cali,[26] M. Calvi,[29,b] M. Calvo Gomez,[43] P. Camargo Magalhaes,[2,h] J. I. Cambon Bouzas,[45] P. Campana,[26] D. H. Campora Perez,[76] A. F. Campoverde Quezada,[7] S. Capelli,[29] L. Capriotti,[24] R. Caravaca-Mora,[9] A. Carbone,[23,i] L. Carcedo Salgado,[45] R. Cardinale,[27,j] A. Cardini,[30] P. Carniti,[29,b] L. Carus,[20] A. Casais Vidal,[63] R. Caspary,[20] G. Casse,[59] J. Castro Godinez,[9] M. Cattaneo,[47] G. Cavallero,[24,47] V. Cavallini,[24,f] S. Celani,[20] D. Cervenkov,[62] S. Cesare,[28,k] A. J. Chadwick,[59] I. Chahrour,[80] M. Charles,[15] Ph. Charpentier,[47] E. Chatzianagnostou,[36] C. A. Chavez Barajas,[59] M. Chefdeville,[10] C. Chen,[12] S. Chen,[5] Z. Chen,[7] A. Chernov,[39] S. Chernyshenko,[51] V. Chobanova,[78] S. Cholak,[48] M. Chrzaszcz,[39] A. Chubykin,[42] V. Chulikov,[42] P. Ciambrone,[26] X. Cid Vidal,[45] G. Ciezarek,[47] P. Cifra,[47] P. E. L. Clarke,[57] M. Clemencic,[47] H. V. Cliff,[54] J. Closier,[47] C. Cocha Toapaxi,[20] V. Coco,[47] J. Cogan,[12] E. Cogneras,[11] L. Cojocariu,[41] P. Collins,[47] T. Colombo,[47] A. Comerma-Montells,[44] L. Congedo,[22] A. Contu,[30] N. Cooke,[58] I. Corredoira,[45] A. Correia,[15] G. Corti,[47] J. J. Cottee Meldrum,[53] B. Couturier,[47] D. C. Craik,[49] M. Cruz Torres,[2,l] E. Curras Rivera,[48] R. Currie,[57] C. L. Da Silva,[66] S. Dadabaev,[42] L. Dai,[69] X. Dai,[6] E. Dall'Occo,[18] J. Dalseno,[45] C. D'Ambrosio,[47] J. Daniel,[11] A. Danilina,[42] P. d'Argent,[22] A. Davidson,[55] J. E. Davies,[61] A. Davis,[61] O. De Aguiar Francisco,[61] C. De Angelis,[30,m] F. De Benedetti,[47] J. de Boer,[36] K. De Bruyn,[75] S. De Capua,[61] M. De Cian,[20,47] U. De Freitas Carneiro Da Graca,[2,n] E. De Lucia,[26] J. M. De Miranda,[2] L. De Paula,[3] M. De Serio,[22,o] P. De Simone,[26] F. De Vellis,[18] J. A. de Vries,[76] F. Debernardis,[22] D. Decamp,[10] V. Dedu,[12] L. Del Buono,[15] B. Delaney,[63] H.-P. Dembinski,[18] J. Deng,[8] V. Denysenko,[49] O. Deschamps,[11] F. Dettori,[30,m] B. Dey,[74] P. Di Nezza,[26] I. Diachkov,[42] S. Didenko,[42] S. Ding,[67] L. Dittmann,[20] V. Dobishuk,[51] A. D. Docheva,[58] C. Dong,[4] A. M. Donohoe,[21] F. Dordei,[30] A. C. dos Reis,[2] A. D. Dowling,[67] W. Duan,[70] P. Duda,[77] M. W. Dudek,[39] L. Dufour,[47] V. Duk,[32] P. Durante,[47] M. M. Duras,[77] J. M. Durham,[66] O. D. Durmus,[74] A. Dziurda,[39] A. Dzyuba,[42] S. Easo,[56] E. Eckstein,[17] U. Egede,[1] A. Egorychev,[42] V. Egorychev,[42] S. Eisenhardt,[57] E. Ejopu,[61] L. Eklund,[79] M. Elashri,[64] J. Ellbracht,[18] S. Ely,[60] A. Ene,[41] E. Epple,[64] J. Eschle,[67] S. Esen,[20] T. Evans,[61] F. Fabiano,[30,m] L. N. Falcao,[2] Y. Fan,[7] B. Fang,[72] L. Fantini,[32,47,p] M. Faria,[48] K. Farmer,[57] D. Fazzini,[29,b] L. Felkowski,[77] M. Feng,[5,7] M. Feo,[18,47] M. Fernandez Gomez,[45] A. D. Fernez,[65] F. Ferrari,[23] F. Ferreira Rodrigues,[3] M. Ferrillo,[49] M. Ferro-Luzzi,[47] S. Filippov,[42] R. A. Fini,[22] M. Fiorini,[24,f] K. L. Fischer,[62] D. S. Fitzgerald,[80] C. Fitzpatrick,[61] F. Fleuret,[14] M. Fontana,[23] L. F. Foreman,[61] R. Forty,[47] D. Foulds-Holt,[54] M. Franco Sevilla,[65] M. Frank,[47] E. Franzoso,[24,f] G. Frau,[61] C. Frei,[47] D. A. Friday,[61] J. Fu,[7] Q. Fuehring,[18] Y. Fujii,[1] T. Fulghesu,[15] E. Gabriel,[36] G. Galati,[22] M. D. Galati,[36] A. Gallas Torreira,[45] D. Galli,[23,i] S. Gambetta,[57] M. Gandelman,[3] P. Gandini,[28] B. Ganie,[61] H. Gao,[7] R. Gao,[62] Y. Gao,[8] Y. Gao,[6] Y. Gao,[8] M. Garau,[30,m] L. M. Garcia Martin,[48] P. Garcia Moreno,[44] J. García Pardiñas,[47] K. G. Garg,[8] L. Garrido,[44] C. Gaspar,[47] R. E. Geertsema,[36] L. L. Gerken,[18] E. Gersabeck,[61] M. Gersabeck,[61] T. Gershon,[55] Z. Ghorbanimoghaddam,[53] L. Giambastiani,[31,g] F. I. Giasemis,[15,q] V. Gibson,[54] H. K. Giemza,[40] A. L. Gilman,[62] M. Giovannetti,[26] A. Gioventù,[44] P. Gironella Gironell,[44] C. Giugliano,[24,f] M. A. Giza,[39] E. L. Gkougkousis,[60] F. C. Glaser,[13,20] V. V. Gligorov,[15,47] C. Göbel,[68] E. Golobardes,[43] D. Golubkov,[42]

A. Golutvin,[60,42,47] A. Gomes,[2,a,r] S. Gomez Fernandez,[44] F. Goncalves Abrantes,[62] M. Goncerz,[39] G. Gong,[4] J. A. Gooding,[18] I. V. Gorelov,[42] C. Gotti,[29] J. P. Grabowski,[17] L. A. Granado Cardoso,[47] E. Graugés,[44] E. Graverini,[48,s] L. Grazette,[55] G. Graziani, A. T. Grecu,[41] L. M. Greeven,[36] N. A. Grieser,[64] L. Grillo,[58] S. Gromov,[42] C. Gu,[14] M. Guarise,[24] M. Guittiere,[13] V. Guliaeva,[42] P. A. Günther,[20] A.-K. Guseinov,[48] E. Gushchin,[42] Y. Guz,[6,42,47] T. Gys,[47] K. Habermann,[17] T. Hadavizadeh,[1] C. Hadjivasiliou,[65] G. Haefeli,[48] C. Haen,[47] J. Haimberger,[47] M. Hajheidari,[47] M. M. Halvorsen,[47] P. M. Hamilton,[65] J. Hammerich,[59] Q. Han,[8] X. Han,[20] S. Hansmann-Menzemer,[20] L. Hao,[7] N. Harnew,[62] M. Hartmann,[13] J. He,[7,t] F. Hemmer,[47] C. Henderson,[64] R. D. L. Henderson,[1,55] A. M. Hennequin,[47] K. Hennessy,[59] L. Henry,[48] J. Herd,[60] P. Herrero Gascon,[20] J. Heuel,[16] A. Hicheur,[3] G. Hijano Mendizabal,[49] D. Hill,[48] S. E. Hollitt,[18] J. Horswill,[61] R. Hou,[8] Y. Hou,[11] N. Howarth,[59] J. Hu,[20] J. Hu,[70] W. Hu,[6] X. Hu,[4] W. Huang,[7] W. Hulsbergen,[36] R. J. Hunter,[55] M. Hushchyn,[42] D. Hutchcroft,[59] D. Ilin,[42] P. Ilten,[64] A. Inglessi,[42] A. Iniukhin,[42] A. Ishteev,[42] K. Ivshin,[42] R. Jacobsson,[47] H. Jage,[16] S. J. Jaimes Elles,[46,73] S. Jakobsen,[47] E. Jans,[36] B. K. Jashal,[46] A. Jawahery,[65,47] V. Jevtic,[18] E. Jiang,[65] X. Jiang,[5,7] Y. Jiang,[7] Y. J. Jiang,[6] M. John,[62] D. Johnson,[52] C. R. Jones,[54] T. P. Jones,[55] S. Joshi,[40] B. Jost,[47] N. Jurik,[47] I. Juszczak,[39] D. Kaminaris,[48] S. Kandybei,[50] Y. Kang,[4] C. Kar,[11] M. Karacson,[47] D. Karpenkov,[42] A. Kauniskangas,[48] J. W. Kautz,[64] F. Keizer,[47] M. Kenzie,[54] T. Ketel,[36] B. Khanji,[67] A. Kharisova,[42] S. Kholodenko,[33,47] G. Khreich,[13] T. Kirn,[16] V. S. Kirsebom,[29,b] O. Kitouni,[63] S. Klaver,[37] N. Kleijne,[33,e] K. Klimaszewski,[40] M. R. Kmiec,[40] S. Koliiev,[51] L. Kolk,[18] A. Konoplyannikov,[42] P. Kopciewicz,[38,47] P. Koppenburg,[36] M. Korolev,[42] I. Kostiuk,[36] O. Kot,[51] S. Kotriakhova, A. Kozachuk,[42] P. Kravchenko,[42] L. Kravchuk,[42] M. Kreps,[55] P. Krokovny,[42] W. Krupa,[67] W. Krzemien,[40] O. K. Kshyvanskyi,[51] J. Kubat,[20] S. Kubis,[77] M. Kucharczyk,[39] V. Kudryavtsev,[42] E. Kulikova,[42] A. Kupsc,[79] B. K. Kutsenko,[12] D. Lacarrere,[47] A. Lai,[30] A. Lampis,[30] D. Lancierini,[54] C. Landesa Gomez,[45] J. J. Lane,[1] R. Lane,[53] C. Langenbruch,[20] J. Langer,[18] O. Lantwin,[42] T. Latham,[55] F. Lazzari,[33,s] C. Lazzeroni,[52] R. Le Gac,[12] R. Lefèvre,[11] A. Leflat,[42] S. Legotin,[42] M. Lehuraux,[55] E. Lemos Cid,[47] O. Leroy,[12] T. Lesiak,[39] B. Leverington,[20] A. Li,[4] H. Li,[70] K. Li,[8] L. Li,[61] P. Li,[47] P.-R. Li,[71] Q. Li,[5,7] S. Li,[8] T. Li,[5,u] T. Li,[70] Y. Li,[8] Y. Li,[5] Z. Lian,[4] X. Liang,[67] S. Libralon,[46] C. Lin,[7] T. Lin,[56] R. Lindner,[47] V. Lisovskyi,[48] R. Litvinov,[30,47] F. L. Liu,[1] G. Liu,[70] K. Liu,[71] S. Liu,[5,7] Y. Liu,[57] Y. Liu,[71] Y. L. Liu,[60] A. Lobo Salvia,[44] A. Loi,[30] J. Lomba Castro,[45] T. Long,[54] J. H. Lopes,[3] A. Lopez Huertas,[44] S. López Soliño,[45] C. Lucarelli,[25,d] D. Lucchesi,[31,g] M. Lucio Martinez,[76] V. Lukashenko,[36,51] Y. Luo,[6] A. Lupato,[31] E. Luppi,[24,f] K. Lynch,[21] X.-R. Lyu,[7] G. M. Ma,[4] R. Ma,[7] S. Maccolini,[18] F. Machefert,[13] F. Maciuc,[41] B. Mack,[67] I. Mackay,[62] L. M. Mackey,[67] L. R. Madhan Mohan,[54] M. J. Madurai,[52] A. Maevskiy,[42] D. Magdalinski,[36] D. Maisuzenko,[42] M. W. Majewski,[38] J. J. Malczewski,[39] S. Malde,[62] L. Malentacca,[47] A. Malinin,[42] T. Maltsev,[42] G. Manca,[30,m] G. Mancinelli,[12] C. Mancuso,[28,13,k] R. Manera Escalero,[44] D. Manuzzi,[23] D. Marangotto,[28,k] J. F. Marchand,[10] R. Marchevski,[48] U. Marconi,[23] S. Mariani,[47] C. Marin Benito,[44] J. Marks,[20] A. M. Marshall,[53] G. Martelli,[32,p] G. Martellotti,[34] L. Martinazzoli,[47] M. Martinelli,[29,b] D. Martinez Santos,[45] F. Martinez Vidal,[46] A. Massafferri,[2] R. Matev,[47] A. Mathad,[47] V. Matiunin,[42] C. Matteuzzi,[67] K. R. Mattioli,[14] A. Mauri,[60] E. Maurice,[14] J. Mauricio,[44] P. Mayencourt,[48] M. Mazurek,[40] M. McCann,[60] L. Mcconnell,[21] T. H. McGrath,[61] N. T. McHugh,[58] A. McNab,[61] R. McNulty,[21] B. Meadows,[64] G. Meier,[18] D. Melnychuk,[40] F. M. Meng,[4] M. Merk,[36,76] A. Merli,[48] L. Meyer Garcia,[65] D. Miao,[5,7] H. Miao,[7] M. Mikhasenko,[17,v] D. A. Milanes,[73] A. Minotti,[29,b] E. Minucci,[67] T. Miralles,[11] B. Mitreska,[18] D. S. Mitzel,[18] A. Modak,[56] A. Mödden,[18] R. A. Mohammed,[62] R. D. Moise,[16] S. Mokhnenko,[42] T. Mombächer,[47] M. Monk,[55,1] S. Monteil,[11] A. Morcillo Gomez,[45] G. Morello,[26] M. J. Morello,[33,e] M. P. Morgenthaler,[20] A. B. Morris,[47] A. G. Morris,[12] R. Mountain,[67] H. Mu,[4] Z. M. Mu,[6] E. Muhammad,[55] F. Muheim,[57] M. Mulder,[75] K. Müller,[49] F. Muñoz-Rojas,[9] R. Murta,[60] P. Naik,[59] T. Nakada,[48] R. Nandakumar,[56] T. Nanut,[47] I. Nasteva,[3] M. Needham,[57] N. Neri,[28,k] S. Neubert,[17] N. Neufeld,[47] P. Neustroev,[42] J. Nicolini,[18,13] D. Nicotra,[76] E. M. Niel,[48] N. Nikitin,[42] P. Nogarolli,[3] P. Nogga,[17] N. S. Nolte,[63] C. Normand,[53] J. Novoa Fernandez,[45] G. Nowak,[64] C. Nunez,[80] H. N. Nur,[58] A. Oblakowska-Mucha,[38] V. Obraztsov,[42] T. Oeser,[16] S. Okamura,[24,f] A. Okhotnikov,[42] O. Okhrimenko,[51] R. Oldeman,[30,m] F. Oliva,[57] M. Olocco,[18] C. J. G. Onderwater,[76] R. H. O'Neil,[57] J. M. Otalora Goicochea,[3] P. Owen,[49] A. Oyanguren,[46] O. Ozcelik,[57] K. O. Padeken,[17] B. Pagare,[55] P. R. Pais,[20] T. Pajero,[47] A. Palano,[22] M. Palutan,[26] G. Panshin,[42] L. Paolucci,[55] A. Papanestis,[56]

M. Pappagallo,[22,o] L. L. Pappalardo,[24,f] C. Pappenheimer,[64] C. Parkes,[61] B. Passalacqua,[24] G. Passaleva,[25] D. Passaro,[33,e] A. Pastore,[22] M. Patel,[60] J. Patoc,[62] C. Patrignani,[23,i] A. Paul,[67] C. J. Pawley,[76] A. Pellegrino,[36] J. Peng,[5,7] M. Pepe Altarelli,[26] S. Perazzini,[23] D. Pereima,[42] H. Pereira Da Costa,[66] A. Pereiro Castro,[45] P. Perret,[11] A. Perro,[47] K. Petridis,[53] A. Petrolini,[27,j] J. P. Pfaller,[64] H. Pham,[67] L. Pica,[33,e] M. Piccini,[32] B. Pietrzyk,[10] G. Pietrzyk,[13] D. Pinci,[34] F. Pisani,[47] M. Pizzichemi,[29,47,b] V. Placinta,[41] M. Plo Casasus,[45] F. Polci,[15,47] M. Poli Lener,[26] A. Poluektov,[12] N. Polukhina,[42] I. Polyakov,[47] E. Polycarpo,[3] S. Ponce,[47] D. Popov,[7] S. Poslavskii,[42] K. Prasanth,[57] C. Prouve,[45] V. Pugatch,[51] G. Punzi,[33,s] S. Qasim,[49] Q. Q. Qian,[6] W. Qian,[7] N. Qin,[4] S. Qu,[4] R. Quagliani,[47] R. I. Rabadan Trejo,[55] J. H. Rademacker,[53] M. Rama,[33] M. Ramírez García,[80] V. Ramos De Oliveira,[68] M. Ramos Pernas,[55] M. S. Rangel,[3] F. Ratnikov,[42] G. Raven,[37] M. Rebollo De Miguel,[46] F. Redi,[28,w] J. Reich,[53] F. Reiss,[61] Z. Ren,[7] P. K. Resmi,[62] R. Ribatti,[48] G. R. Ricart,[14,81] D. Riccardi,[33,e] S. Ricciardi,[56] K. Richardson,[63] M. Richardson-Slipper,[57] K. Rinnert,[59] P. Robbe,[13] G. Robertson,[58] E. Rodrigues,[59] E. Rodriguez Fernandez,[45] J. A. Rodriguez Lopez,[73] E. Rodriguez Rodriguez,[45] A. Rogovskiy,[56] D. L. Rolf,[47] P. Roloff,[47] V. Romanovskiy,[42] M. Romero Lamas,[45] A. Romero Vidal,[45] G. Romolini,[24] F. Ronchetti,[48] T. Rong,[6] M. Rotondo,[26] S. R. Roy,[20] M. S. Rudolph,[67] M. Ruiz Diaz,[20] R. A. Ruiz Fernandez,[45] J. Ruiz Vidal,[79,x] A. Ryzhikov,[42] J. Ryzka,[38] J. J. Saavedra-Arias,[9] J. J. Saborido Silva,[45] R. Sadek,[14] N. Sagidova,[42] D. Sahoo,[74] N. Sahoo,[52] B. Saitta,[30,m] M. Salomoni,[29,47,b] C. Sanchez Gras,[36] I. Sanderswood,[46] R. Santacesaria,[34] C. Santamarina Rios,[45] M. Santimaria,[26,47] L. Santoro,[2] E. Santovetti,[35] A. Saputi,[24,47] D. Saranin,[42] A. Sarnatskiy,[75] G. Sarpis,[57] M. Sarpis,[61] C. Satriano,[34,y] A. Satta,[35] M. Saur,[6] D. Savrina,[42] H. Sazak,[16] F. Sborzacchi,[47,26] L. G. Scantlebury Smead,[62] A. Scarabotto,[18] S. Schael,[16] S. Scherl,[59] M. Schiller,[58] H. Schindler,[47] M. Schmelling,[19] B. Schmidt,[47] S. Schmitt,[16] H. Schmitz,[17] O. Schneider,[48] A. Schopper,[47] N. Schulte,[18] S. Schulte,[48] M. H. Schune,[13] R. Schwemmer,[47] G. Schwering,[16] B. Sciascia,[26] A. Sciuccati,[47] S. Sellam,[45] A. Semennikov,[42] T. Senger,[49] M. Senghi Soares,[37] A. Sergi,[27,j] N. Serra,[49] L. Sestini,[31] A. Seuthe,[18] Y. Shang,[6] D. M. Shangase,[80] M. Shapkin,[42] R. S. Sharma,[67] I. Shchemerov,[42] L. Shchutska,[48] T. Shears,[59] L. Shekhtman,[42] Z. Shen,[6] S. Sheng,[5,7] V. Shevchenko,[42] B. Shi,[7] Q. Shi,[7] Y. Shimizu,[13] E. Shmanin,[42] R. Shorkin,[42] J. D. Shupperd,[67] R. Silva Coutinho,[67] G. Simi,[31,g] S. Simone,[22,o] N. Skidmore,[55] T. Skwarnicki,[67] M. W. Slater,[52] J. C. Smallwood,[62] E. Smith,[63] K. Smith,[66] M. Smith,[60] A. Snoch,[36] L. Soares Lavra,[57] M. D. Sokoloff,[64] F. J. P. Soler,[58] A. Solomin,[42,53] A. Solovev,[42] I. Solovyev,[42] R. Song,[1] Y. Song,[48] Y. Song,[4] Y. S. Song,[6] F. L. Souza De Almeida,[67] B. Souza De Paula,[3] E. Spadaro Norella,[28,k] E. Spedicato,[23] J. G. Speer,[18] E. Spiridenkov,[42] P. Spradlin,[58] V. Sriskaran,[47] F. Stagni,[47] M. Stahl,[47] S. Stahl,[47] S. Stanislaus,[62] E. N. Stein,[47] O. Steinkamp,[49] O. Stenyakin,[42] H. Stevens,[18] D. Strekalina,[42] Y. Su,[7] F. Suljik,[62] J. Sun,[30] L. Sun,[72] Y. Sun,[65] D. Sundfeld,[2] W. Sutcliffe,[49] P. N. Swallow,[52] F. Swystun,[54] A. Szabelski,[40] T. Szumlak,[38] Y. Tan,[4] M. D. Tat,[62] A. Terentev,[42] F. Terzuoli,[33,47,z] F. Teubert,[47] E. Thomas,[47] D. J. D. Thompson,[52] H. Tilquin,[60] V. Tisserand,[11] S. T'Jampens,[10] M. Tobin,[5,47] L. Tomassetti,[24,f] G. Tonani,[28,47,k] X. Tong,[6] D. Torres Machado,[2] L. Toscano,[18] D. Y. Tou,[4] C. Trippl,[43] G. Tuci,[20] N. Tuning,[36] L. H. Uecker,[20] A. Ukleja,[38] D. J. Unverzagt,[20] E. Ursov,[42] A. Usachov,[37] A. Ustyuzhanin,[42] U. Uwer,[20] V. Vagnoni,[23] G. Valenti,[23] N. Valls Canudas,[47] H. Van Hecke,[66] E. van Herwijnen,[60] C. B. Van Hulse,[45,aa] R. Van Laak,[48] M. van Veghel,[36] G. Vasquez,[49] R. Vazquez Gomez,[44] P. Vazquez Regueiro,[45] C. Vázquez Sierra,[45] S. Vecchi,[24] J. J. Velthuis,[53] M. Veltri,[25,bb] A. Venkateswaran,[48] M. Vesterinen,[55] M. Vieites Diaz,[47] X. Vilasis-Cardona,[43] E. Vilella Figueras,[59] A. Villa,[23] P. Vincent,[15] F. C. Volle,[52] D. vom Bruch,[12] N. Voropaev,[42] K. Vos,[76] G. Vouters,[10,47] C. Vrahas,[57] J. Wagner,[18] J. Walsh,[33] E. J. Walton,[1,55] G. Wan,[6] C. Wang,[20] G. Wang,[8] J. Wang,[6] J. Wang,[5] J. Wang,[4] J. Wang,[72] M. Wang,[28] N. W. Wang,[7] R. Wang,[53] X. Wang,[8] X. Wang,[70] X. W. Wang,[60] Y. Wang,[6] Z. Wang,[13] Z. Wang,[4] Z. Wang,[28] J. A. Ward,[55,1] M. Waterlaat,[47] N. K. Watson,[52] D. Websdale,[60] Y. Wei,[6] J. Wendel,[78] B. D. C. Westhenry,[53] D. J. White,[61] M. Whitehead,[58] A. R. Wiederhold,[55] D. Wiedner,[18] G. Wilkinson,[62] M. K. Wilkinson,[64] M. Williams,[63] M. R. J. Williams,[57] R. Williams,[54] F. F. Wilson,[56] W. Wislicki,[40] M. Witek,[39] L. Witola,[20] C. P. Wong,[66] G. Wormser,[13] S. A. Wotton,[54] H. Wu,[67] J. Wu,[8] Y. Wu,[6] Z. Wu,[7] K. Wyllie,[47] S. Xian,[70] Z. Xiang,[5] Y. Xie,[8] A. Xu,[33] J. Xu,[7] L. Xu,[4] L. Xu,[4] M. Xu,[55] Z. Xu,[11] Z. Xu,[7] Z. Xu,[5] D. Yang,[4] K. Yang,[60] S. Yang,[7] X. Yang,[6] Y. Yang,[27,j] Z. Yang,[6] Z. Yang,[65] V. Yeroshenko,[13] H. Yeung,[61] H. Yin,[8] C. Y. Yu,[6] J. Yu,[69] X. Yuan,[5] E. Zaffaroni,[48] M. Zavertyaev,[19] M. Zdybal,[39] C. Zeng,[5,7] M. Zeng,[4]

C. Zhang,[6] D. Zhang,[8] J. Zhang,[7] L. Zhang,[4] S. Zhang,[69] S. Zhang,[6] Y. Zhang,[6] Y. Z. Zhang,[4] Y. Zhao,[20] A. Zharkova,[42] A. Zhelezov,[20] S. Z. Zheng,[6] X. Z. Zheng,[4] Y. Zheng,[7] T. Zhou,[6] X. Zhou,[8] Y. Zhou,[7] V. Zhovkovska,[55] L. Z. Zhu,[7] X. Zhu,[4] X. Zhu,[8] V. Zhukov,[16] J. Zhuo,[46] Q. Zou,[5,7] D. Zuliani,[31,g] and G. Zunica[48]

(LHCb Collaboration)

[1]*School of Physics and Astronomy, Monash University, Melbourne, Australia*
[2]*Centro Brasileiro de Pesquisas Físicas (CBPF), Rio de Janeiro, Brazil*
[3]*Universidade Federal do Rio de Janeiro (UFRJ), Rio de Janeiro, Brazil*
[4]*Center for High Energy Physics, Tsinghua University, Beijing, China*
[5]*Institute of High Energy Physics (IHEP), Beijing, China*
[6]*School of Physics State Key Laboratory of Nuclear Physics and Technology, Peking University, Beijing, China*
[7]*University of Chinese Academy of Sciences, Beijing, China*
[8]*Institute of Particle Physics, Central China Normal University, Wuhan, Hubei, China*
[9]*Consejo Nacional de Rectores (CONARE), San Jose, Costa Rica*
[10]*Université Savoie Mont Blanc, CNRS, IN2P3-LAPP, Annecy, France*
[11]*Université Clermont Auvergne, CNRS/IN2P3, LPC, Clermont-Ferrand, France*
[12]*Aix Marseille Université, CNRS/IN2P3, CPPM, Marseille, France*
[13]*Université Paris-Saclay, CNRS/IN2P3, IJCLab, Orsay, France*
[14]*Laboratoire Leprince-Ringuet, CNRS/IN2P3, Ecole Polytechnique, Institut Polytechnique de Paris, Palaiseau, France*
[15]*LPNHE, Sorbonne Université, Paris Diderot Sorbonne Paris Cité, CNRS/IN2P3, Paris, France*
[16]*I. Physikalisches Institut, RWTH Aachen University, Aachen, Germany*
[17]*Universität Bonn—Helmholtz-Institut für Strahlen und Kernphysik, Bonn, Germany*
[18]*Fakultät Physik, Technische Universität Dortmund, Dortmund, Germany*
[19]*Max-Planck-Institut für Kernphysik (MPIK), Heidelberg, Germany*
[20]*Physikalisches Institut, Ruprecht-Karls-Universität Heidelberg, Heidelberg, Germany*
[21]*School of Physics, University College Dublin, Dublin, Ireland*
[22]*INFN Sezione di Bari, Bari, Italy*
[23]*INFN Sezione di Bologna, Bologna, Italy*
[24]*INFN Sezione di Ferrara, Ferrara, Italy*
[25]*INFN Sezione di Firenze, Firenze, Italy*
[26]*INFN Laboratori Nazionali di Frascati, Frascati, Italy*
[27]*INFN Sezione di Genova, Genova, Italy*
[28]*INFN Sezione di Milano, Milano, Italy*
[29]*INFN Sezione di Milano-Bicocca, Milano, Italy*
[30]*INFN Sezione di Cagliari, Monserrato, Italy*
[31]*INFN Sezione di Padova, Padova, Italy*
[32]*INFN Sezione di Perugia, Perugia, Italy*
[33]*INFN Sezione di Pisa, Pisa, Italy*
[34]*INFN Sezione di Roma La Sapienza, Roma, Italy*
[35]*INFN Sezione di Roma Tor Vergata, Roma, Italy*
[36]*Nikhef National Institute for Subatomic Physics, Amsterdam, Netherlands*
[37]*Nikhef National Institute for Subatomic Physics and VU University Amsterdam, Amsterdam, Netherlands*
[38]*AGH—University of Krakow, Faculty of Physics and Applied Computer Science, Kraków, Poland*
[39]*Henryk Niewodniczanski Institute of Nuclear Physics Polish Academy of Sciences, Kraków, Poland*
[40]*National Center for Nuclear Research (NCBJ), Warsaw, Poland*
[41]*Horia Hulubei National Institute of Physics and Nuclear Engineering, Bucharest-Magurele, Romania*
[42]*Affiliated with an institute covered by a cooperation agreement with CERN*
[43]*DS4DS, La Salle, Universitat Ramon Llull, Barcelona, Spain*
[44]*ICCUB, Universitat de Barcelona, Barcelona, Spain*
[45]*Instituto Galego de Física de Altas Enerxías (IGFAE), Universidade de Santiago de Compostela, Santiago de Compostela, Spain*
[46]*Instituto de Fisica Corpuscular, Centro Mixto Universidad de Valencia—CSIC, Valencia, Spain*
[47]*European Organization for Nuclear Research (CERN), Geneva, Switzerland*
[48]*Institute of Physics, Ecole Polytechnique Fédérale de Lausanne (EPFL), Lausanne, Switzerland*
[49]*Physik-Institut, Universität Zürich, Zürich, Switzerland*

[50]*NSC Kharkiv Institute of Physics and Technology (NSC KIPT), Kharkiv, Ukraine*
[51]*Institute for Nuclear Research of the National Academy of Sciences (KINR), Kyiv, Ukraine*
[52]*School of Physics and Astronomy, University of Birmingham, Birmingham, United Kingdom*
[53]*H.H. Wills Physics Laboratory, University of Bristol, Bristol, United Kingdom*
[54]*Cavendish Laboratory, University of Cambridge, Cambridge, United Kingdom*
[55]*Department of Physics, University of Warwick, Coventry, United Kingdom*
[56]*STFC Rutherford Appleton Laboratory, Didcot, United Kingdom*
[57]*School of Physics and Astronomy, University of Edinburgh, Edinburgh, United Kingdom*
[58]*School of Physics and Astronomy, University of Glasgow, Glasgow, United Kingdom*
[59]*Oliver Lodge Laboratory, University of Liverpool, Liverpool, United Kingdom*
[60]*Imperial College London, London, United Kingdom*
[61]*Department of Physics and Astronomy, University of Manchester, Manchester, United Kingdom*
[62]*Department of Physics, University of Oxford, Oxford, United Kingdom*
[63]*Massachusetts Institute of Technology, Cambridge, Massachusetts, USA*
[64]*University of Cincinnati, Cincinnati, Ohio, USA*
[65]*University of Maryland, College Park, Maryland, USA*
[66]*Los Alamos National Laboratory (LANL), Los Alamos, New Mexico, USA*
[67]*Syracuse University, Syracuse, New York, USA*
[68]*Pontifícia Universidade Católica do Rio de Janeiro (PUC-Rio), Rio de Janeiro, Brazil (associated with Universidade Federal do Rio de Janeiro (UFRJ), Rio de Janeiro, Brazil)*
[69]*School of Physics and Electronics, Hunan University, Changsha City, China (associated with Institute of Particle Physics, Central China Normal University, Wuhan, Hubei, China)*
[70]*Guangdong Provincial Key Laboratory of Nuclear Science, Guangdong-Hong Kong Joint Laboratory of Quantum Matter, Institute of Quantum Matter, South China Normal University, Guangzhou, China (associated with Center for High Energy Physics, Tsinghua University, Beijing, China)*
[71]*Lanzhou University, Lanzhou, China (associated with Institute of High Energy Physics (IHEP), Beijing, China)*
[72]*School of Physics and Technology, Wuhan University, Wuhan, China (associated with Center for High Energy Physics, Tsinghua University, Beijing, China)*
[73]*Departamento de Fisica, Universidad Nacional de Colombia, Bogota, Colombia (associated with LPNHE, Sorbonne Université, Paris Diderot Sorbonne Paris Cité, CNRS/IN2P3, Paris, France)*
[74]*Eotvos Lorand University, Budapest, Hungary (associated with European Organization for Nuclear Research (CERN), Geneva, Switzerland)*
[75]*Van Swinderen Institute, University of Groningen, Groningen, Netherlands (associated with Nikhef National Institute for Subatomic Physics, Amsterdam, Netherlands)*
[76]*Universiteit Maastricht, Maastricht, Netherlands (associated with Nikhef National Institute for Subatomic Physics, Amsterdam, Netherlands)*
[77]*Tadeusz Kosciuszko Cracow University of Technology, Cracow, Poland (associated with Henryk Niewodniczanski Institute of Nuclear Physics Polish Academy of Sciences, Kraków, Poland)*
[78]*Universidade da Coruña, A Coruña, Spain (associated with DS4DS, La Salle, Universitat Ramon Llull, Barcelona, Spain)*
[79]*Department of Physics and Astronomy, Uppsala University, Uppsala, Sweden (associated with School of Physics and Astronomy, University of Glasgow, Glasgow, United Kingdom)*
[80]*University of Michigan, Ann Arbor, MI, United States (associated with Syracuse University, Syracuse, New York, USA)*
[81]*Département de Physique Nucléaire (DPhN), Gif-Sur-Yvette, France*

[a]Deceased.
[b]Also at Università degli Studi di Milano-Bicocca, Milano, Italy.
[c]Also at Università di Roma Tor Vergata, Roma, Italy.
[d]Also at Università di Firenze, Firenze, Italy.
[e]Also at Scuola Normale Superiore, Pisa, Italy.
[f]Also at Università di Ferrara, Ferrara, Italy.
[g]Also at Università di Padova, Padova, Italy.
[h]Also at Facultad de Ciencias Fisicas, Madrid, Spain.
[i]Also at Università di Bologna, Bologna, Italy.
[j]Also at Università di Genova, Genova, Italy.
[k]Also at Università degli Studi di Milano, Milano, Italy.
[l]Also at Universidad Nacional Autónoma de Honduras, Tegucigalpa, Honduras.
[m]Also at Università di Cagliari, Cagliari, Italy.

[n]Also at Centro Federal de Educacão Tecnológica Celso Suckow da Fonseca, Rio De Janeiro, Brazil.
[o]Also at Università di Bari, Bari, Italy.
[p]Also at Università di Perugia, Perugia, Italy.
[q]Also at LIP6, Sorbonne Université, Paris, France.
[r]Also at Universidade de Brasília, Brasília, Brazil.
[s]Also at Università di Pisa, Pisa, Italy.
[t]Also at Hangzhou Institute for Advanced Study, UCAS, Hangzhou, China.
[u]Also at School of Physics and Electronics, Henan University, Kaifeng, China.
[v]Also at Excellence Cluster ORIGINS, Munich, Germany.
[w]Also at Università di Bergamo, Bergamo, Italy.
[x]Also at Department of Physics/Division of Particle Physics, Lund, Sweden.
[y]Also at Università della Basilicata, Potenza, Italy.
[z]Also at Università di Siena, Siena, Italy.
[aa]Also at Universidad de Alcalá, Alcalá de Henares, Spain.
[bb]Also at Università di Urbino, Urbino, Italy.